A STUDY ON GAS EVOLVING ELECTRODES UNDER EXTREME CURRENT DENSITIES

Zahra Ghorbani

A thesis

In the Department of

Mechanical and Industrial Engineering

Presented in Partial Fulfillment of the Requirements

For the Degree of

Master of Applied Science (Mechanical Engineering) at

Concordia University

Montréal, Québec, Canada

February 2012

CONCORDIA UNIVERSITY
School of Graduate Studies

This is to certify that the thesis prepared

By: Zahra Ghorbani

Entitled: A Study on Gas Evolving Electrodes under Extreme Current Densities

and submitted in partial fulfillment of the requirements for the degree of

Master of Applied Science (Mechanical Engineering)

complies with the regulations of the University and meets the accepted standards with respect to originality and quality.

Signed by the final examining committee:

Dr. Lyse Kadem Chair

Dr. Ali Dolatabadi Examiner

Dr. Fariborz Haghighat Examiner

Dr. Rolf Wuthrich and Dr. Marius Paraschivoiu Supervisor

Approved by

Chair of Department or Graduate Program Director

Dean of Faculty

Date

ABSTRACT

A Study on Gas Evolving Electrodes under Extreme Current Densities

Zahra Ghorbani

Electrochemical discharges or electrode effects are used in different fields such as micro-machining, nano-particle production, and surface engineering. Further development and improvement of the different applications of electrochemical discharges require a better understanding of this process. Beyond the critical voltage, an insulating gas film forms around the electrode and discharges take place through the gas film. The stability of the gas film affects the quality of the discharges. The gas film formation is therefore investigated in the present thesis.

The main objective of the current project is to attain a better insight into the gas film dynamics. This goal is achieved through the following approaches: 1. The current-voltage characteristics are studied prior to the gas film formation and then compared with a model developed based on the percolation theory. 2. Since the hydrodynamic forces define the shape and thickness of the gas film, the effect of the hydrodynamic parameters on a gas film are analyzed. Based on the Pi theorem and dimensional analysis, important dimensionless parameters are derived to investigate the gas film formation. 3. Different system configurations are examined to improve the electrochemical discharge activity. Visual observations indicate that stable discharges are obtained by using a covered electrode and applying an offset pulsed voltage.

Key words: Electrochemical discharges, Gas film formation time, Gas film thickness, Gas bubble evolution

Acknowledgements

It is a pleasure to thank the many people who made this thesis possible. Firstly, I would like to express my most sincere gratitude to my supervisor, Dr. Rolf Wüthrich. I gratefully appreciate his continuous support to my Master's studies, his patience, motivation, and most tremendous knowledge in the matter. His consistent guidance helped me complete this research and write this thesis.

I am deeply grateful to Dr. Marius Paraschivoiu for his supervision, kindness, and constructive comments. He helped me at all levels of my research project and provided thoughtful advice.

Moreover, I would like to thank my oral defense committee members: Dr. Ali Dolatabadi and Dr. Fariborz Haghighat for their time, insightful questions, and helpful comments.

I am very grateful to Dr. Ali Dolatabadi, Dr. Lyse Kadem, and their research groups for their assistance and collaboration. Sincere thanks to Julio and Emmanuel for their help in running my setup.

I would also like to thank my colleagues at the Electro-catalytic green engineering lab who have contributed immensely to my personal and professional growth. I am especially grateful to Anis, Andrew, Farzad and Maniya. They have proven to be supportive friends as well as thoughtful colleagues with good advice and collaboration.

I wish to thank my friends for their emotional support especially my best friend Sanam for helping me get through difficult times and for the caring she has provided always. I also thank Carole for proofreading my thesis.

Finally, my deepest and most heartfelt thank you to my family: My parents who provided the best possible environment for me to grow up and supported me in all my pursuits, my husband, Farzad, for his unconditional love and his faith in me, and my sisters and brothers for all their love and encouragement. To them I dedicate this thesis.

Zahra Ghorbani
Concordia University
February 2012

Contents

List of Figures

List of Tables

List of Symbols

Latin Symbols

A	Electrode surface	m^2
A	Experimental constant	1
a_i	Activity of species i	1
B	Experimental constant	1
b	Electrode radius	m
c	Specific heat	J/kg.K
d	Bubble layer thickness	m
d_f	Gas film thickness	m
E	Electrical field	V/m
e	Electron charge magnitude	C
F	Faraday's constant	C/mol
Fr	Froude number	1
g	Acceleration due to gravity	m/s^2
h	Electrode immersion depth	m
I	Electrical current	A
I_0	Electrical current without bubble layer	A
I_∞	Electrical current with bubble layer	A
$\bar{I}$	Normalized current	1
j	Current density	A/m^2
j_o	Exchange current density	A/m^2
k	Electrolyte conductivity	1/Ω.m
L	Length	m
N	Number of nucleation sites	1
N_G	flux to bubbles adhering to the electrode	mol/s
N_E	flux to the bulk of electrolyte	mol/s
N_F	flux of gas evolved in bulk	mol/s
N_O	flux of dissolved gas removed from the inter-electrode gap	mol/s
n_s	Normalized cluster number	1
P	Pressure	Pa
P	Probability	1
p	Mean occupation probability of the lattice site	1
p_c	Percolation thershold	1
P_i	Partial pressure of gas i	Pa
R	Universal gas constant	J/mol K

R	Electrical resistance	Ω
R	Bubble diameter	m
R_o	Resistance of the electrolyte without bubble layer	Ω
R_∞	Resistance of the electrolyte with bubble layer	Ω
r	Radius	m
Re	Reynolds number	1
s	Cluster size	1
T	Temperature	K
t	time	s
t_f	Gas film formation time	s
$\bar{t}$	Normalized time	1
U	Terminal voltage	V
U_o	Terminal voltage at thermodynamic equilibrium	V
U_d	Water decomposition potential	V
$\overline{U}$	Normalized Voltage	1
V	Velocity	m/s
$\dot{V}_G$	Amount of gas produced per time	m^3/s
V_b	Mean bubble volume	m^3
We	Weber number	1
z	Number of ion charges	1

Greek Symbols

α	Symmetry factor	1
β	Coefficient of Faradic gas generation	m^3/A
Δt_b	Bubble detachment time	s
ε	Mean gas void fraction	1
η	Over-potential	V
θ	Bubble coverage fraction	1
θ_c	Critical bubble coverage fraction	1
λ	Thermal conductivity	W/m.K
λ_d	Probability of gas discharges	$1/m^2.s$
μ	Viscosity	kg/m.s
μ_i	Chemical potential of species i	J/mol
μ_i^o	Chemical potential of chemical species i under standard condition	J/mol
ν	Stoichiometric number	1

ξd_n	Mean bubble height	m
ρ	Mass density	Kg/m^3
σ	Surface tension	N/m
ϕ	Electrostatic potential	V
Ω	Lateral tool surface	m^2

Subscripts

a	anode
c	cathode
eff	effective

Superscripts

$crit$	Critical
$diff$	Diffusion
lim	limit
max	maximal

1. INTRODUCTION

A two-electrode cell consists of two electrodes dipped into an electrolyte (Figure **1**). Conventional electrolysis occurs as long as the current density is small (typically smaller than 1A/mm^2). When the cell terminal is higher than a critical voltage (such that the current density exceeds 1 A/mm^2), the electrolysis is no longer sustained and the so-called electrochemical discharges (ECD) phenomenon occurs. This phenomenon takes place because the bubbles around the electrode form an insulating film. Consequently, electrical discharges with light emission occur through the gas film. The electrochemical discharges have been known since the nineteenth century. Different engineering applications have been reported for this phenomenon, such as surface engineering [1], waste water treatment [2], nano-particle production [3,4], micro machining of non-conductive materials [5,6,7], reduction of metal salts and high frequency current interrupters.

Several applications would benefit from conducting a thorough investigation of the fundamental mechanism governing electrochemical discharges thereby providing additional insight to the current knowledge. For example, the interpretation of the current signal during the ECD phenomenon presents good potential to provide new insights into the gas film dynamics and the resulting discharges. The latter is the aim of the current study.

1.1.Problem Statement

Further development of the different practical applications of ECD requires a better understanding of this process. The desire to understand ECD has led to many studies in the last 150 years [8]. However, there is no generally accepted explanation for the physical and chemical mechanisms involved in the ECD process.

The onset of the ECD is the formation of an insulating gas film [9, 47]. This gas film has an unpredictable behavior that makes it challenging to study. The dynamic properties and the stability of the gas film have a direct impact on the practical applications. For example, in machining applications, the unstable gas film yields fluctuations in the electrochemical discharges which result in a low repeatability of the process, subsequently deteriorating the machining quality [10]. In nano-particle production by ECD an unstable gas film yields unstable discharges and, consequently, inhomogeneous nano-particles. The present thesis aims to provide a better understanding of the fundamental mechanisms governing ECD and identify the main parameters influencing this process.

1.2.Motivation and Challenges

Literature review has shown that there are no generally accepted results characterizing the fundamental mechanisms governing ECD. Studying the ECD phenomenon is challenging because of its complexity and unpredictability. The main objective of this project is to get a better insight into the gas film dynamics.

Due to the complexity and the stochastic nature of ECD, the present thesis relies on experimental studies. The experimental visualization of the process is deemed as a most

efficient approach to achieve the thesis objective. In effect, it is found that literature lacks researches that are based on such an experimental technique.

This study has been divided into three parts:

1. The different regions of the current-voltage characteristics were analyzed based on the current signal and corresponding video images captured with a high speed camera. The experimental results are compared with a model, based on percolation theory, which predicts the current-voltage characteristics before the formation of the gas film.

2. The study of the characteristics of the gas film, such as the gas film thickness and the gas film formation time is a necessity to improve the industrial applications of ECD. The gas film thickness and the gas film formation time were measured based on the images captured.

3. The effect of the concentration of the electrolyte and capillary forces on the gas film characteristics has not yet been reported in literature and is conducted in the present study.

4. A stable gas film is a precondition in order to have repeatable ECD and optimize their applications. A new system configuration was designed and consists of covering the electrode and applying an offset pulsed voltage to obtain a stable gas film.

The main challenges in visualizing and analyzing the experimental data are as follows:

a. The thickness of the gas film is in the range of micrometers and the gas film formation time is in the range of milliseconds which implies that a high speed camera is required for high quality images.

b. Effective visualization requires a suitable cell, solution and light.

c. The nature of the data obtained from the cell is stochastic which makes the data analysis challenging.

1.3.Contributions

The main contributions of the current thesis work are the following:

1. It is found that the properties of the solution have a great influence on the gas film parameters. The gas film formation time decreases exponentially as the voltage increases. Moreover, the concentration has a great effect on the gas film thickness and the gas film formation time. The results obtained can be used to improve the gas film quality and consequently the ECD quality.

2. The theoretical model developed by Wüthrich [32] is validated experimentally.

3. Repeatable electrochemical discharges using a covered electrode and a pulse voltage are achieved.

4. Reynolds and Weber numbers are determined as fundamental dimensionless parameters for the analysis of the gas film in ECD.

2. ELECTROCHEMICAL DISCHARGES

2.1. Fundamentals

To understand the electrochemical discharges, elementary electrochemistry knowledge is necessary. In this section, a brief description of the fundamentals of electrochemistry is given. The electrolysis phenomenon happens when an electric potential is applied between two electrodes that are immersed in an electrolyte. For example, in alkaline solutions at the cathode, the following reactions occur consecutively, and hydrogen is produced:

1) Volmer reaction :

$$\boldsymbol{M + H_2O + e^- \rightarrow M - H_{ads} + OH^-} \tag{2.1}$$

Followed by the

2) Heyrovsky reaction

$$\boldsymbol{M - H_{ads} + M + H_2O + e^- \rightarrow 2M + H_2 + OH^-} \tag{2.2}$$

or

Tafel reaction

$$\boldsymbol{M - H_{ads} + M - H_{ads} \rightarrow 2M + H_2} \tag{2.3}$$

where $M - H_{ads}$ represents the hydrogen adsorbed on the electrode.

At the anode, chemical reactions result in oxygen evolution. Reactions at the anode are more complicated. In an alkalin solution the overall reaction is:

$$\boldsymbol{4OH^- \rightarrow O_2 + 2H_2O + 4e^-} \tag{2.4}$$

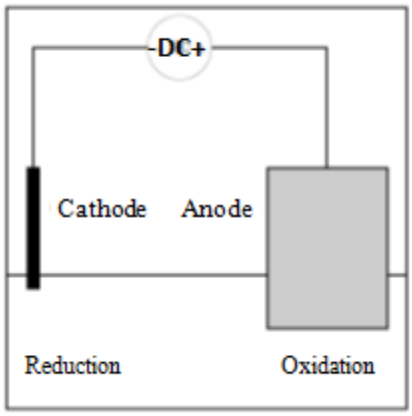

Figure 1- Two electrode cell

2.2. Potential Distribution in an Electrochemical Cell

Thermodynamic equilibrium for an electrode dipped into a solution is represented as:

$$\mu_i(metal) = \mu_i(solution) \tag{2.5}$$

where μ_i is the chemical potential of the chemical species i and is given by

$$\mu_i = \mu_i^0 + RTln(a_i) \tag{2.6}$$

with R the universal gas constant (8.3145 J/mol K), T the temperature of the system (in Kelvin) and a_i the activity of the chemical species.

When an electrode is inserted in an electrolyte, at first the system is not in thermodynamic equilibrium. It moves toward equilibrium by exchanging electrons between the electrode and the electrolyte.

$$M \rightleftharpoons M^{z+} + ze^- \tag{2.7}$$

This means that metal from the electrode dissolves to the electrolyte or metal from the electrolyte deposits onto the electrode.

The potential difference that appears between electrode and electrolyte is related to the species in the solution and can be represented by the Nernst equation:

$$\Delta\phi_0 = \Delta\phi_{00} + \frac{RT}{zF} ln a_{M^{z+}} \tag{2.8}$$

where z is the charge number of species and F is the Faraday constant (the magnitude of electric charge per mole of electrons = 96,485.3365(21) (C/mol). $\Delta\phi_{00}$ in the above equation is defined as:

$$\Delta\phi_{00} = \frac{\mu^0_{M^{z+}} + \mu^0_M}{zF} \tag{2.9}$$

where μ_i^0represents the chemical potential of species i under standard conditions.

Nernst equation also can be derived for other reactions. For example for the general redox reaction:

$$Ox + ze^- \rightleftharpoons Red \tag{2.10}$$

Nernst equation is

$$\phi_0 = \phi_{00} + \frac{RT}{zF} ln \frac{a_{Red}}{a_{Ox}} \tag{2.11}$$

according to a fixed standard reference.

For the hydrogen evolution reaction at the gas evolving electrode

$$2H_3O^+ + 2e^- \rightleftharpoons H_2 + H_2O \tag{2.12}$$

Nernst equation can be written as

$$\phi_0 = \phi_{00} + \frac{RT}{F} ln \frac{a_{H_3O^+}}{\sqrt{P_{H_2}}} \tag{2.13}$$

where $P_{H_2}$is the partial pressure of H_2. The reference is fixed by choosing the activity of water $a_{H_2O} = 1$.

In a typical two electrode cell as shown in Figure 1, electron transfer takes place at the electrode. The electric equivalent circuit of this cell is shown in Figure 2. R_1 and R_2 are

the charge transfer resistances at the electrodes and R_0 is the electrolyte resistance. R_0 depends on the electrolyte conductivity and the cell geometry. Electrolyte conductivity is originated from the ionic conductivity of the charged ions in the electrolyte. The electrochemical processes at the electrodes, because of the charge transfers, result in nonlinear resistances in function of the current at the electrodes (R_1 and R_2).

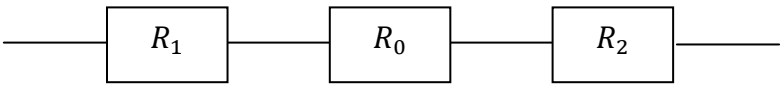

Figure 2- Electric circuit equivalent to cell shown in Figure1

These electrochemical reactions at the electrodes are:

$$\boldsymbol{X + ze^- \rightleftharpoons X_{red}} \tag{2.14}$$

$$\boldsymbol{Y \rightleftharpoons Y_{ox} + ze^-} \tag{2.15}$$

Equation 2.14 is called a reduction reaction and equation 2.15 is called an oxidation reaction.

The potential difference between the two electrodes is called terminal voltage and is measured as:

$$\boldsymbol{U = \phi^1 - \phi^2} \tag{2.16}$$

As already discussed, this voltage can be measured by the Nernst equation when the cell is at thermodynamic equilibrium. Nernst equation for a two-electrode cell is

$$\boldsymbol{U_0 = \phi^1_{00} - \phi^2_{00} - \frac{RT}{zF}\ln\left(\frac{a_{X_{red}} a_{Y_{ox}}}{a_X a_Y}\right)} \tag{2.17}$$

When the cell is connected to a power source, electrolysis happens; the electrical current drives the system away from equilibrium and the electrode potentials change. This system is called electrochemical cell.

The system can also be driven away from the equilibrium state by connecting it to an external charge. This makes the system move towards a new equilibrium in which both electrodes have the same potential. This kind of system is called a galvanic cell. The evolution of the cell voltage with the current for electrochemical and galvanic cells is represented in Figure 3.

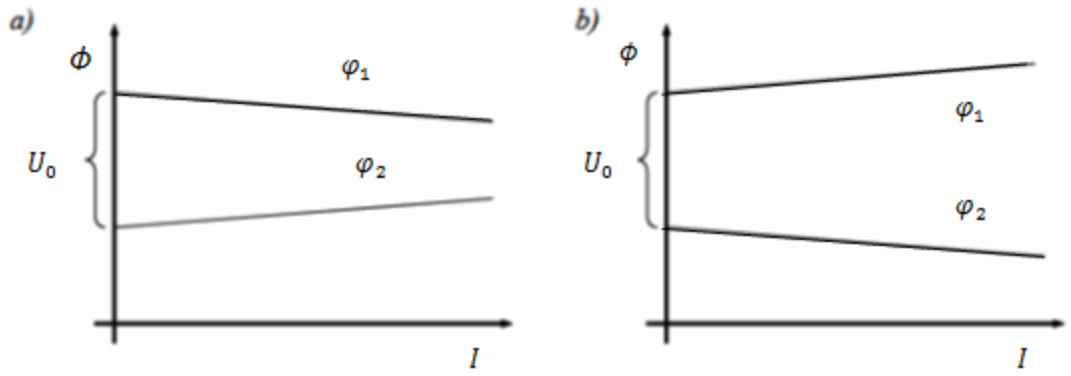

Figure 3- Evolution of potential with current, a) galvanic cell b) electrochemical cell

Note that the potential of an electrode changes when it is connected to an external current. The difference between the potential of the electrode and the potential of the electrode at thermodynamic equilibrium is called the over-potential, and denoted η:

$$\boldsymbol{\eta = \phi - \phi_0} \tag{2.18}$$

The over-potential controls the electrochemical reactions. The terminal voltage of a cell can be expressed as:

$$\boldsymbol{U = U_0 + \sum |\eta| + R_0 I} \tag{2.19}$$

where $R_0 I$ is the ohmic drop that occurs due to the resistance of the electrolyte. In equation 2.19, the potentials are considered to be positive at the anode, where the electrons are transferred from the electrolyte to the electrode, and negative at the cathode, where the electrons are transferred from the electrode to the electrolyte.

The Butler-Volmer equation describes the relation between the over potential η and the current density j:

$$\boldsymbol{j(\eta) = j_0 \left(\exp\left[\frac{(1-\alpha)zF}{RT}\eta\right] - \exp\left[-\frac{\alpha zF}{RT}\eta\right]\right)} \tag{2.20}$$

where j_0 is the exchange current density in $[{}^{A}/_{m^2}]$. In applications where the current density is high, considering equation 2.20, the over-potential can be expressed as a constant value and independent of the current density. Therefore, equation 2.19 can be re-written as:

$$\boldsymbol{U = U_d + R_0 I} \tag{2.21}$$

$$\boldsymbol{U_d = U_0 + \sum |\eta|} \tag{2.22}$$

The definition of U_d, the so-called water decomposition potential, is illustrated in Figure 4.

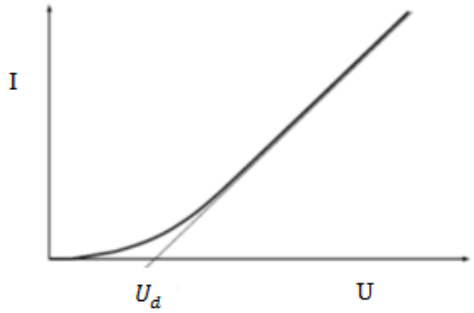

Figure 4- Definition of water decomposition potential

2.3.Bubble Formation at a Gas Evolving Electrode

The surface of an electrode contains nucleation sites such as pits, scratches and cavities which hold trapped gas. The trapped gases grow as the interface between the electrode-electrolyte becomes supersaturated with dissolved gas.

As an example, during water electrolysis, hydrogen evolves at the electrode in a dissolved form.

$$2H^+ + 2e^- \rightleftharpoons H_2(dissolved) \tag{2.23}$$

At low current densities, the dissolved product is transferred to the bulk by diffusion. At high current densities, the concentration of the dissolved gas at the electrode-electrolyte interface increases, which results in activating more nucleation sites. The dissolved hydrogen in the vicinity of the electrode produces hydrogen in gas phase forming a bubble:

$$H_2(dissolved) \rightleftharpoons H_2(bubble) \tag{2.24}$$

Part of the gaseous hydrogen attaches to the bubbles at the surface of the electrode. Part of it diffuses to the electrolyte bulk where it either attaches to the moving bubbles or leaves the inter-electrode gap (Figure 5) [11]. The region where the bubbles adhere to the electrode surface is called the adherence region. When the bubbles leave the electrode, they diffuse into the diffusion region. There exists another region called the bulk region that contains a few dispersed bubbles. It is observed that some bubbles jump directly from the adherence region to the bulk region [12]. Figure 6 shows the three different regions around a gas evolving electrode.

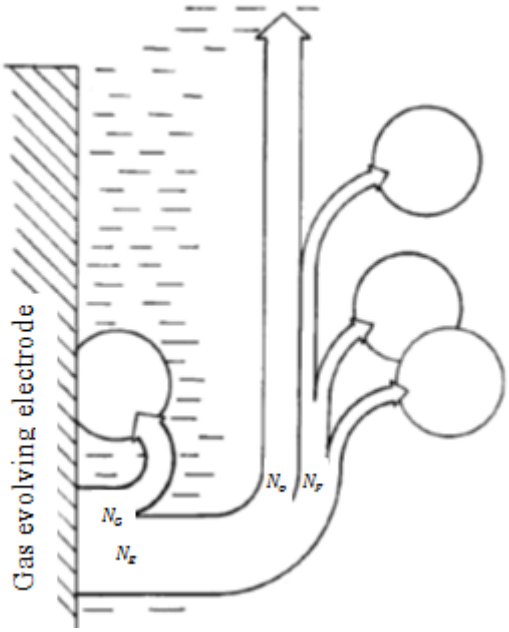

Figure 5- Flow of dissolved gas N_G to bubbles at the electrode surface , N_O out of the inter-electrode gap and N_F to the bubbles in the bulk electrolyte, reprinted from [11] with permission from Springer.

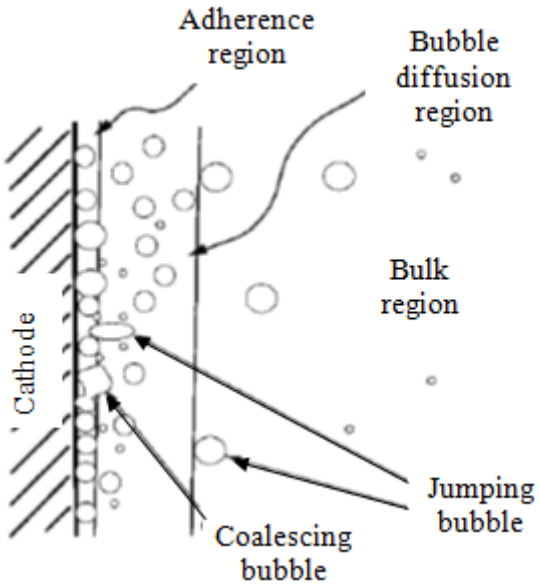

Figure 6- Bubble layer structure around a gas evolving electrode, reprinted from [12] with permission from Springer

When a bubble detaches from the electrode, the nucleation sites become supersaturated with the dissolved gas, subsequently forming another bubble, and repeating the same cycle.

The newly formed bubble may either coalesce or slide along the electrode, and then leave the surface of the electrode. Two forces act on the bubble, buoyancy and capillary. When these forces are equal in magnitude, the bubble detaches from the electrode [7]. The departure radius of the bubbles depends on different parameters such as the surface roughness and wettability of the electrode and the concentration and pH of the electrolyte. The departure radius of the bubble is independent of the current density when the latter is high, and dependent on the current density when the latter is low [7].

The growing bubbles change the inter-electrode resistance. They cover some parts of the electrode and reduce the active electrode area. The fraction of the electrode covered by the bubbles is represented by θ. The current density, I/A increases when the active area decreases. The local current density of an electrode of a surface A covered by bubbles is given by:

$$\boldsymbol{j_{local} = \frac{1}{1-\theta}\frac{I}{A}} \tag{2.25}$$

where I is the current through the electrode of surface A.

The bubbles in the inter-electrode gap increase the resistance of the electrolyte. Several relations are used in the electrochemical literatures to quantify the electrochemical conductivity of the electrolyte. The most widely used are Bruggeman relation [13]

$$\boldsymbol{k_{eff} = k(1-\varepsilon)^{\frac{3}{2}}} \tag{2.26}$$

and Maxwell's relation [14]:

$$\boldsymbol{k_{eff} = k(1 + 1.5\frac{\varepsilon}{1-\varepsilon})^{-1}} \tag{2.27}$$

In the above relations, ε is the gas void fraction which represents the fraction of the volume of gas over the total volume of gas and liquid. k is the conductivity of the electrolyte without bubbles. These relations give almost the same result as shown in Figure 7.

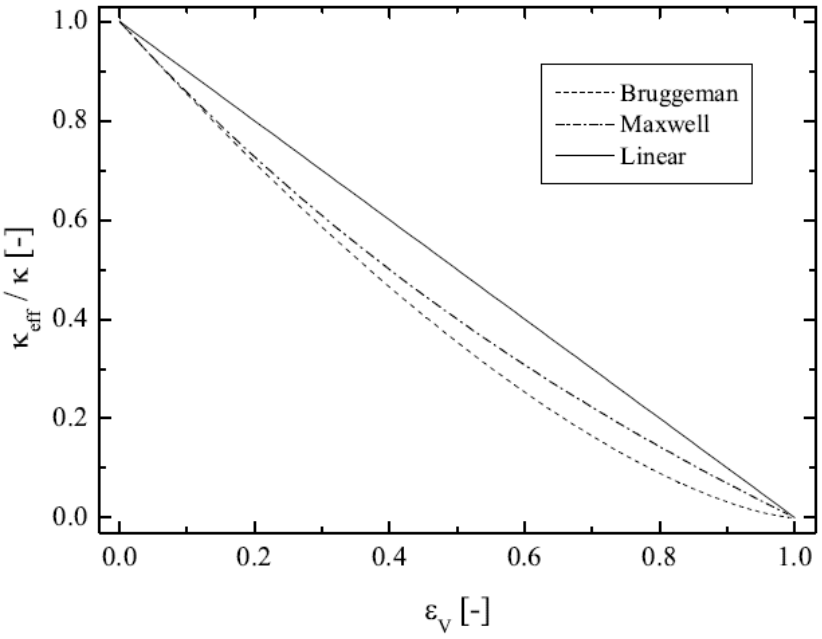

Figure 7- Relative conductivity $\frac{k_{eff}}{k}$ of an electrolyte as a function of the gas void fraction ε [7]

The existence of bubbles adds a supplementary potential drop to equation 2.19. [7]:

$$\boldsymbol{U = U_0 + |\eta_a| + |\eta_c| + R^{bulk}I + \frac{R^{diff}}{1-\theta}I} \tag{2.28}$$

where R^{diff} is the resistance of the bubble diffusion region and can be calculated using the Bruggeman relation. For example, considering a cylindrical electrode of radius b and height h surrounded by bubble diffusion region of thickness d, length h, and radius b, R^{diff} for this specific electrode is:

$$R^{diff}(\varepsilon) = \frac{1}{(1-\varepsilon)^{3/2}} \frac{1}{2\pi kh} \ln\left(\frac{b+d}{b}\right) \quad (2.29)$$

The schematic potential distribution around a gas evolving electrode is represented in Figure 8. The current density is much larger at the working electrode as the latter has a smaller surface area. The large fraction of the potential drop at the working electrode is due to the bubble layer formed around this electrode as a result of high current density.

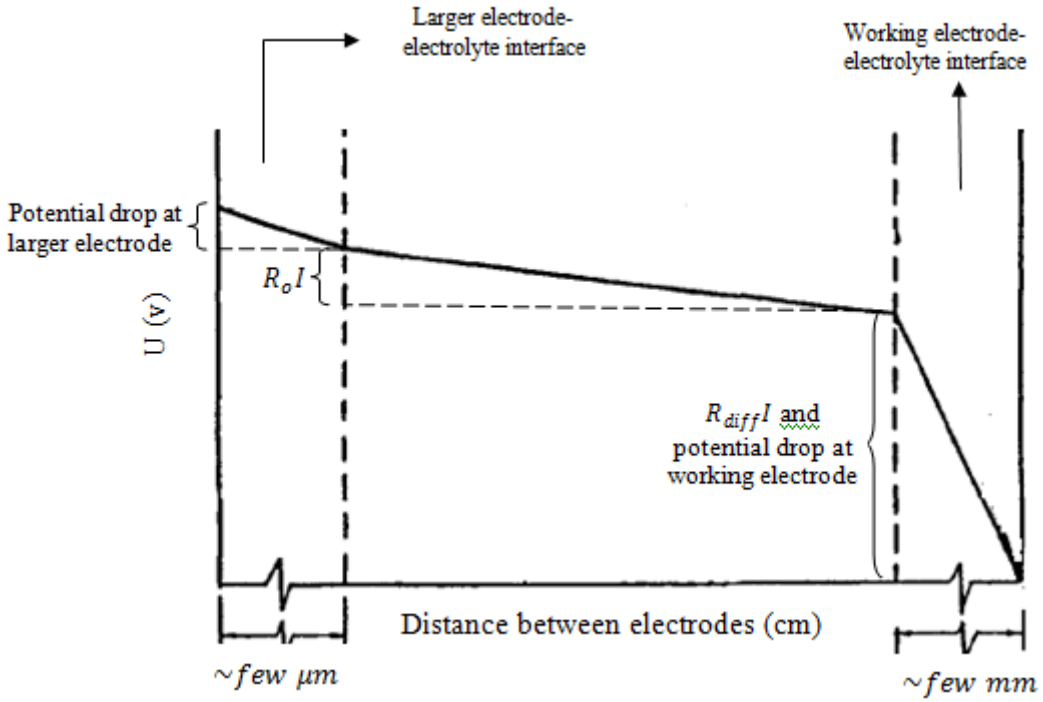

Figure 8- Potential distribution around a gas evolving electrode [55]

2.4.Bubble Coalescence

When two bubbles collide, the interface between them becomes thinner. If they are in contact for a time longer than the critical coalescence time, the interface ruptures and the two bubbles coalesce [17]. The critical coalescence time depends on the bubble size and

the properties of the interface between the two bubbles, such as the viscosity of the liquid and the surface tension.

The critical coalescence time is related to the surface tension. It is reported in [15] that the bubbles coalesce if the Weber number ($We = \frac{\rho V^2 R}{\sigma}$) is below 0.18. Therefore, the bubble coalescence rate changes by adding surfactants. The viscosity of the electrolyte affects as well the coalescence of the bubbles. It is shown that the higher the viscosity of the electrolyte, the easier the bubbles interact with each other and the more likely the bubbles coalesce [16]. Furthermore, the average size of the bubbles has a strong effect on the coalescence of the bubbles. It is shown [17] for different solutions that as the bubble size is increased the rate of coalescence decreases.

2.5.Current-Voltage Characteristics of an Electrochemical Cell

Figure 9 shows the typical current-voltage characteristics of an electrochemical cell. Six different regimes are identified [18,19] in this plot:

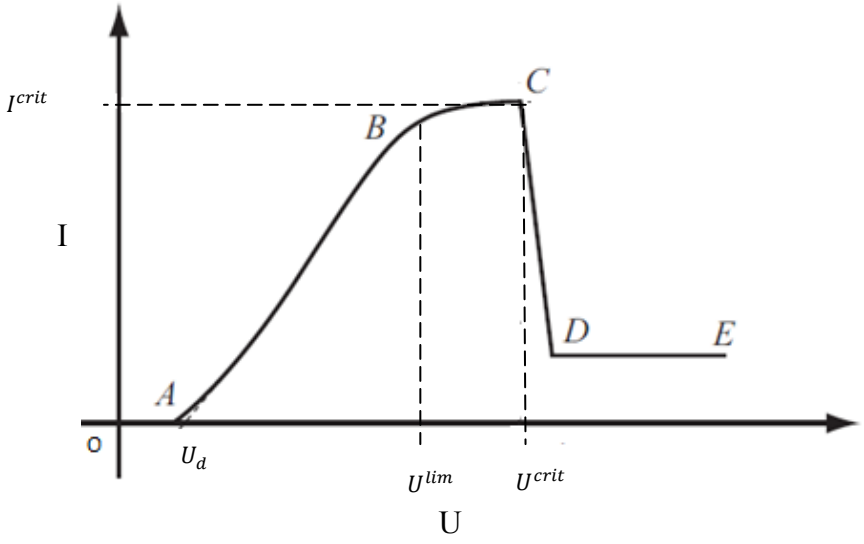

Figure 9- Typical I-U characteristics of an electrochemical cell

- OA, 0 < U < U_d, thermodynamic region: No electrolysis occurs in this region. No current is flowing through the cell.
- AB, U_d< U < U^{lim}, ohmic region: The traditional electrolysis takes place. The current increases almost linearly with the voltage. This behavior is due to the ohmic resistance of the electrolyte.
- BC, U^{lim} < U < U^{crit}, limiting current region: In this region the bubbles are coalescing and the bubble coverage fraction increases. The voltage at which the current drops suddenly is called the critical voltage U^{crit} and the corresponding current is the critical current I^{crit}. In the limiting region, the current reaches its maximum and remains constant as the voltage increases.
- CD, U^{crit} < U < 1.2 U^{crit}, transition region: A compact gas film covers the electrode progressively.
- DE, 1.2 U^{crit} < U: A gas film blankets the electrode. The discharges are the only path allowing the current to flow. Water vapor is also generated in this region because of the high temperature of the electrode.
- Another region is mentioned by Fascio et al. [18] and is located between OA and AB. In this region, there is a slight change in the current because of the high over-potential of hydrogen evolution reaction at the electrode.

2.6.Gas Film

Beyond the critical voltage, the growing bubbles around the electrode coalesce and form a gas film that insulates the electrode. This phenomenon is known in the electrochemical literature as the electrode effect. Although this effect has been known for over 150 years

[8], an explanation for the sudden change occurring from the electrolysis to the gas film formation remains a controversial topic. Several mechanisms have been considered as reasons leading to the gas film formation including local electrolyte evaporation by Joule heating, hydrodynamic and wettability effects, as well as electrochemically formed gas bubbles.

Kellogg [20] showed that the gas film formation in ECD is similar to gas film formation around a hot wire when inserted in water. He believed that the gas film is primarily a water vapor film and it forms when the electrode temperature, due to Joule heating, reaches the boiling temperature of the electrolyte. Beside the experiments that he conducted to prove his idea, Kellogg calculated the heat dissipated from the electrode in ECD and hot wire and showed good agreement between the two approaches. He proposed that the high pressure of the electrolyte vapor keeps the electrolyte away from the electrode. The gas film tends to break due to the hydrostatic forces that are present as the electrolyte approaches the electrode. However, the electrolyte vaporizes and is pushed away from the electrode. He discussed the vibration of the gas film as a result of this behavior. When the film is in proximity of the electrode surface, gas ionization takes place due to the existing high potential gradient. When the latter is intense enough, a visible discharge occurs.

Many other researchers [21,22,23,24] believe that local evaporation is one of the mechanisms leading to gas film formation. Klupathy [23] derived an equation, based on this hypothesis, for the gas film formation time:

$$t_f = k\rho c\left(\frac{RA}{U - U_d}\right)^2 (T_e - T_o) \tag{2.30}$$

where k is the electrical conductivity of the electrolyte (measured in 1/Ω), ρ is the electrolyte density (in kg/m^3), c is the specific heat of the electrolyte (in J/kg.K) , R is the inter-electrode resistance (in Ω), A is the surface of the electrode (in m^2), U is the cell terminal voltage (in V), U_d is the water decomposition potential (in V), T_e is the evaporation temperature of the electrolyte, and T_o is the initial temperature of the electrolyte (in K).

Wüthrich [7] derived a more precise relation by considering the heat transfer through the electrolyte:

$$\frac{\mathbf{1}}{\overline{\boldsymbol{r}}}\frac{\boldsymbol{\partial}}{\boldsymbol{\partial}\overline{\boldsymbol{r}}}\left(\overline{\boldsymbol{r}}\frac{\boldsymbol{\partial}\overline{\boldsymbol{T}}}{\boldsymbol{\partial}\overline{\boldsymbol{r}}}\right)+\frac{\boldsymbol{K}}{\overline{\boldsymbol{r}}^{\boldsymbol{2}}}=\frac{\boldsymbol{\partial}\overline{\boldsymbol{T}}}{\boldsymbol{\partial}\overline{\boldsymbol{t}}}, \tag{2.31}$$

where $\overline{r}$ is the normalized distance, $\frac{r}{b}$ (where b is the electrode radius), $\overline{T}$ is the normalized temperature, $\frac{T}{T_0}$ and $\overline{t}$ is the normalized time, $\frac{t}{\tau}$. τ is a time constant defined as:

$$\boldsymbol{\tau}=\frac{\boldsymbol{\rho c}}{\boldsymbol{\lambda}}\boldsymbol{b}^{\boldsymbol{2}} \tag{2.32}$$

where λ is the thermal conductivity of the electrode (in W/m.K).

K is a constant defined as:

$$\boldsymbol{K}=\frac{\mathbf{1}}{\boldsymbol{k\lambda}}\left(\frac{\boldsymbol{I}}{\boldsymbol{2\pi h}}\right)^{\mathbf{2}}\frac{\mathbf{1}}{\boldsymbol{T_0}} \tag{2.33}$$

where k is the electrical conductivity of the electrolyte, h is the length of the electrode and T_0 is the initial temperature.

Vogt [25] suggested that the change in the wettability induces the gas film formation. This change may occur because of different reasons such as the concentration of the

electrolyte in the vicinity of the electrode, the electrical charge of the gas-liquid interface, and the electrode material.

Arndt and Probst [26] showed (in the context of the electrolytic aluminum reduction) that the concentration of the electrolyte changes near the electrode and results in a change in the wettability. The change in concentration is attributed to the existence of different active species such as Al^{3+} and Na^{+} [26].

The electrical charge of the gas-liquid interface is another explanation for the change in wettability (in aluminum electrolysis) [28]. During the normal electrolysis, the electrolyte contains sufficient oxygen ions that induce a positive charge on the bubbles and hence get repelled by the anode electrode. As the oxide contents decrease (critical condition in aluminum electrolysis), the electric charge on the gas bubble switches from positive to negative, and the bubbles become electro-statically attracted by the anode. Furthermore, the properties of the electrode material, specially its porosity, have a significant effect on wettability [27].

Mazza et al. [28] explained the phenomenon based on hydrodynamic instabilities described by Helmholtz and Taylor [61,62] which was also considered in the case of boiling. They used cine pictures and studied the critical current density to confirm their findings. They found that the scattering of the critical current density is less for a spherical electrode than a plane electrode [28]. For a spherical electrode, the critical current density is relatively well defined due to the absence of disturbing boundaries. However, in the case of a plane electrode, the presence of disturbing boundaries results in the scattering of the critical current density.

Mazza et al. [28] explained the anode effect in horizontal electrodes as follows: first, bubbles form on the electrode surface, then as the bubbles move upward they form vertical layers of gas with layers of liquid between them. Because of the relative velocity difference existent between the gas layer and the liquid layer, Helmholtz instability causes the boundary surface to break. As a result, a gas film develops to cover the solid surface. At this point, a layer of liquid (heavier fluid) is on the top of the layer of gas (lighter fluid). In this case, the Taylor instability causes the laminar configuration of gas covering the solid surface to collapse.

Wüthrich et al. [29] showed that the electrode effect is attributed to the increasing mean bubble coverage. This effect depends on the ability of the bubble to leave the electrode or coalesce. When the growing bubbles attain a certain size, they cannot leave the electrode due to the capillary forces, and the bubble coverage fraction increases. Wüthrich also presented [9] a model using percolation theory to describe the electrode effect. He applied a theoretical approach to analyze this particular phenomenon. He considered the bubble growth and bubble departure from the electrode to be a stochastic process. The model used the electrolyte concentration and geometrical parameters of the electrode to predict the critical condition inducing the electrode effect. This model is independent of the mechanism governing the gas film formation.

According to Wüthrich [7], decreasing the rate of bubble release and increasing the rate of gas production are additional parameters responsible for the gas film formation. When the bubble detachment time is long enough the gas film can be formed. The viscosity and density of the electrolyte and the wettability of the electrode are the main parameters

affecting the bubble detachment time. The rate of local current density and local joule heating constitute the principal parameters governing the gas production rate.

Basak et al. [30] developed a model that predicts the critical current and voltage. Their model suggests that the critical voltage depends only on the electrolyte concentration and is independent of the electrode geometry. The model ignores some other mechanisms governing the gas film formation; however, it yields results with reasonable accuracy. The model employs the critical resistance value as an input. Wüthrich [9] presented a model that predicts the critical voltage, current, and resistance based on the electrode geometry and the concentration of the electrolyte. This model is described in the following section.

2.7.Gas Film Formation

In this section, the stochastic model developed by Wüthrich [32] to quantify the electrode effect is described. This model is based on percolation theory and explains the transition from the bubble layer to the gas film.

Percolation theory was developed to deal with disordered systems. The main concept of percolation theory is the existence of a sharp transition that occurs at the percolation threshold. The percolation threshold is a critical value at which the connectivity between sub-units of a system appears or disappears.

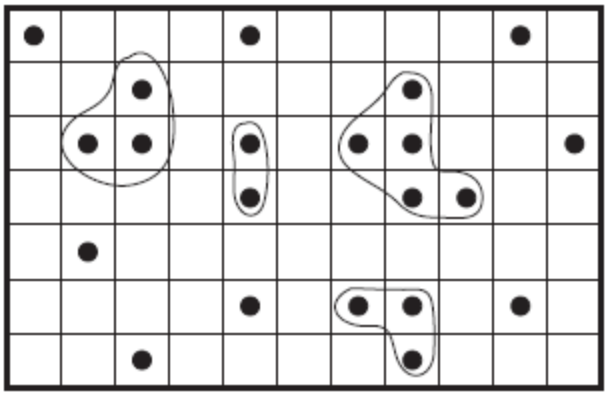

Figure 10- A lateral electrode surface Ω, that presents some sites occupied by the probability p. The neighboring bubbles are assumed to coalesce and form a larger bubble.

Consider a square lattice Ω that has some sites occupied with probability, p (Figure 10). At small values of p, the occupied sites are isolated. If two neighboring sites are occupied, they connect to each other. A group of neighboring occupied sites makes a cluster. As the occupation probability is increased, the number of clusters increases, and some of these clusters may connect to each other. At a critical value of the probability, p_c, an infinite size cluster appears. For any p greater than p_c, the infinite cluster is always present, however, some isolated clusters may exist as well. The infinite cluster grows until every site is occupied, $p = 1$.

Each cluster is characterized by its size, s. The normalized cluster number, n_s, is defined as the number of clusters of size s, per lattice site. Therefore, the probability that an arbitrary lattice site belongs to a cluster with size s is $n_s.s$. $P(p)$ is the probability that one site belongs to the infinite cluster. The following equations give the probability p that an arbitrary site is occupied:

$$\boldsymbol{p = \sum sn_s}, \qquad \boldsymbol{for} \quad \boldsymbol{p \leq p_c} \tag{2.34}$$

$$\boldsymbol{p = \sum s n_s + P(p), \qquad for \quad p > p_c} \tag{2.35}$$

To describe the electrode effect based on percolation theory, Wüthrich idealized the nucleation sites on the electrode. He supposed that Ω is the lateral electrode surface and the nucleation sites are the lattice sites that were introduced by the percolation theory. As one bubble grows, it occupies one lattice site. The bubbles coalesce if they are attached and form a cluster that becomes a new larger bubble. Therefore, in this model, s is the size of a bubble and n_s is the density of the bubbles of size s. p is interpreted as the density of the active nucleation sites or θ. It is assumed that the critical conditions occur when a bubble is not able to leave the electrode. $P(p)$ is defined as the fraction of the electrode covered by a bubble that is not able to leave the electrode or in other words the gas film. This occurs when the bubble is large enough to prevent the buoyancy force from overcoming the adhesion force.

Therefore, when the bubbles are able to leave the electrode, $\theta \leq \theta_c$

$$\boldsymbol{\sum s n_s = \theta} \tag{2.36}$$

and when the bubbles are not able to leave the electrode, $\theta > \theta_c$

$$\boldsymbol{\sum s n_s = \theta - P(\theta)} \tag{2.37}$$

In order to determine the gas film formation time, the mass balance between the amount of gas forming on the electrode and the amount of gas leaving the electrode is written.

The amount of gas bubble produced per unit time can be found from the Faraday's law:

$$\boldsymbol{\dot{V}_G = \beta I} \tag{2.38}$$

where β is the faradic gas generation coefficient and is defined as:

$$\boldsymbol{\beta = \frac{RT}{\left(\frac{z}{\nu}\right) FP}} \tag{2.39}$$

where R is the universal gas constant, T is the temperature, z is the charge number, υ is the stoichiometric number, F is Faraday's constant, and P is the pressure.

Using equation 2.25, equation 2.38 can be written as:

$$\boldsymbol{\dot{V}_G = \beta j_{local}(1-\theta)A} \tag{2.40}$$

The amount of gas leaving the electrode is calculated using the number of bubbles leaving the electrode per unit time. The fraction of the electrode surface that is covered by these bubbles is $\sum_{s=0}^{s^{max}} sn_s(\theta)$, where s^{max} is the maximum size of the bubbles that can leave the electrode. Then, the amount of gas leaving the electrode can be found by

$$\boldsymbol{\dot{V}_G = \frac{V_b}{\Delta t_b} NA \sum_{s=0}^{s^{max}} sn_s(\theta).} \tag{2.41}$$

In equation 2.41, V_b is the mean volume of a bubble that has not yet coalesced with its neighboring bubbles. N is the mean number of nucleation sites per unit area and Δt_b is the bubble detachment time.

The mass balance between the produced gas and the leaving gas gives:

$$\boldsymbol{\frac{d}{dt}(V_b NA\theta) = \beta j_{local}(1-\theta)A - \frac{V_b}{\Delta t_b} NA \sum_{s=0}^{s^{max}} sn_s(\theta)} \tag{2.42}$$

If d_n is the mean distance between two nucleation sites, a gas bubble that has not yet coalesced with its neighboring bubbles presents a height equal to ξd_n. ξ represents the degree of flatness of the bubble and is a function of wettability and the electrode geometry. The volume of one bubble can be approximated by

$$\boldsymbol{V_b = \frac{\xi d_n}{N}}. \tag{2.43}$$

Substituting equation 2.43 into equation 2.42, one can find an equation for the bubble coverage fraction:

$$\boldsymbol{\frac{d}{dt}(\theta) = \frac{\beta j_{local}}{\xi d_n}(1-\theta) - \frac{1}{\Delta t_b}\sum_{s=0}^{s^{max}} s n_s(\theta)} \tag{2.44}$$

The stationary solution of the equation above is:

$$\boldsymbol{\frac{\beta \Delta t_b}{\xi d_n} j_{local}(1-\theta) = \sum_{s=0}^{s^{max}} s n_s(\theta)} \tag{2.45}$$

Considering equations 2.25, 2.36 and 2.45, for $\theta \leq \theta_c$, the stationary bubble coverage fraction can be written as:

$$\boldsymbol{\theta = \frac{\beta \Delta t_b}{\xi d_n}\frac{I}{A}} \tag{2.46}$$

θ is smaller than $\theta_c$as long as the current is smaller than the critical current. The voltage at which the critical current is reached is called the critical voltage. In order to estimate the critical voltage, first, the relation between the cell terminal voltage and the stationary bubble fraction is determined by considering equations 2.21 and 2.46.

$$\boldsymbol{U - U_d = R(\theta) A \frac{\xi d_n}{\beta \Delta t_b}\theta} \tag{2.47}$$

Let $\theta = \theta_c$, the critical voltage becomes:

$$\boldsymbol{U^{crit} = U_d + R(\theta_c) A \frac{\xi d_n}{\beta \Delta t_b}\theta_c} \tag{2.48}$$

By introducing the normalized time

$$\bar{t} = \frac{t}{\Delta t_b} \tag{2.49}$$

And the normalized voltage

$$\bar{U} = \frac{U - U_d}{U^{crit} - U_d}, \tag{2.50}$$

and the normalized current

$$\bar{I} = \frac{I}{I_{crit}} \tag{2.51}$$

and solving equation 2.44 for a step input, the following equation is obtained for a normalized current (Figure 11):

$$\bar{I}(\bar{t}) = \frac{\bar{U}}{1 - \theta_c}\left[1 - \frac{\bar{U}}{\bar{U} + \frac{1 - \theta_c}{\theta_c}}\left(1 - e^{-a\bar{t}}\right)\right] \tag{2.52}$$

where a is

$$a = 1 + \frac{\theta_c}{1 - \theta_c}\bar{U} \tag{2.53}$$

Similarly, t_f, the time needed to reach θ_c, is estimated by solving equation 2.44 for $\bar{t}$ (Figure 12):

$$\bar{t} = \frac{1}{1 + \frac{\theta_c}{1 - \theta_c}\bar{\mathrm{U}}} \ln\left[\frac{\bar{\bar{\mathrm{U}}}}{(1 - \theta_c)(\bar{\mathrm{U}} - 1)}\right] \tag{2.54}$$

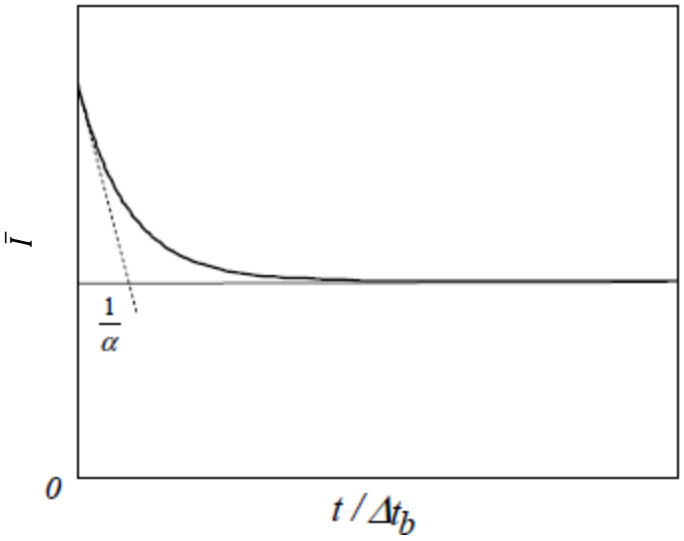

Figure 11- Normalized current for a terminal voltage lower than the critical voltage

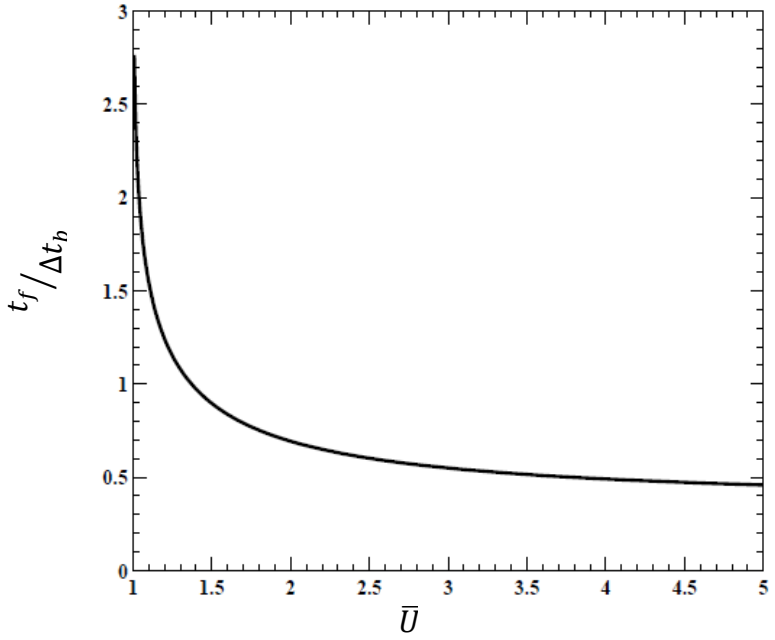

Figure 12- Predicted gas film formation time according to equation 2.55, for the percolation threshold $\theta_c = 0.5$ [7]

2.8.Gas Film Dynamics

Gas film dynamics has been a topic of great interest to researchers in the study of the gas film in the context of ECD. The thickness and gas film formation time are important aspects in the study of gas film dynamics.

The thickness of the gas film for a cylindrical electrode of diameter equal to 1 mm is around 50-100 μm [33]. Different parameters such as the temperature of the electrolyte and the concentration of the electrolyte influence the gas film thickness. The effect of other parameters like wettability of the electrode, applied voltage and capillary has not yet been reported in literature.

The bulk temperature of the electrolyte has a great effect on the gas film thickness [20]. At high temperatures of the electrolyte (around 90℃) the gas film is almost uniform and vibrates slowly. At low temperatures (around 40℃), the gas film vibrates very fast. It means that the gas film waves, shown in Figure 13, move fast and have large amplitude. The gas film is very thin at some parts of the electrode and much thicker at other parts.

The electrolyte concentration has a strong effect on the gas film thickness. $(OH)^-$, which is a hydrophilic ion, increases with increasing electrolyte concentration [34] (for alkaline solutions). Therefore, the wettability changes, and the gas film becomes thinner.

Figure 13- Gas film around an electrode with a 0.5mm diameter Nickel electrode in NaOH 30% at. Gas film waves vibrate slowly at high temperatures and very fast at low temperatures. (See section 5 for details on how image was obtained.)

The mean time needed to form a gas film or gas film formation time is one of the most critical values characterizing gas film dynamics. The gas film formation time, (time t_f that is shown in Figure 14), is about 20 ms [6]. Fascio [35] developed a model that predicts gas film formation time based on the Joule heating effect. The gas film formation time that she obtained was higher than the experimental values. She attributed this discrepancy to the fact that the model underestimates the current density and consequently the heat from the Joule heating effect.

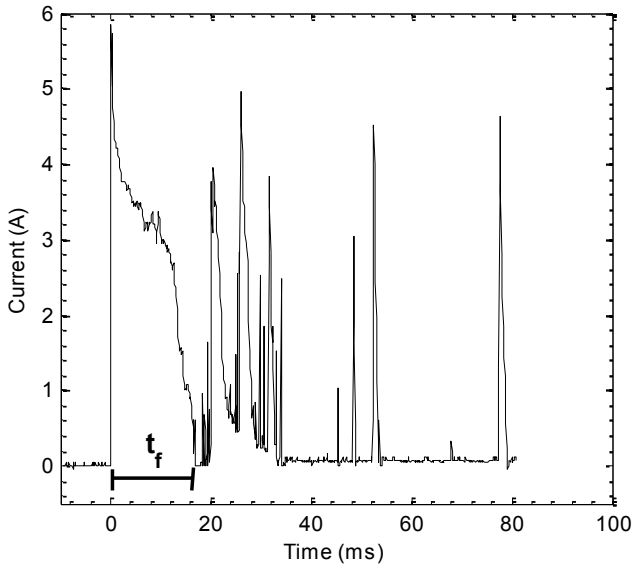

Figure 14- Current signal for a step input of 25 V (higher than the critical voltage). The gas film is formed after a time $t_f = 18\ ms$

Allagui et al. [36] proposed an algorithm to measure the gas film life time and gas film formation time during ECD by analyzing the current-time signal. Moreover, Allagui et al. [36] studied the gas film properties experimentally. They found that the gas film is more stable at higher voltages because of the high temperature of the electrode. Figure 15 is based on their experiments and shows that the gas film formation time decreases and the gas film life time increases as the applied voltage decreases.

At high voltages the production of bubbles is intense. Small and dense bubbles cover the electrode. These bubbles do not coalesce or grow [34]. As a result a dense and thin gas film covers the electrode.

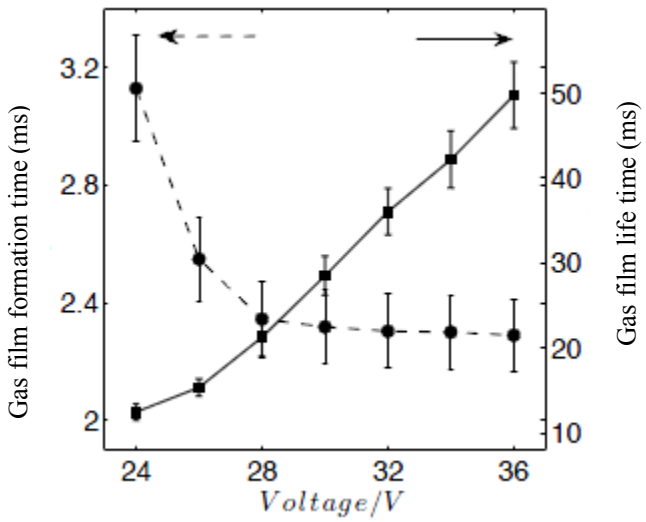

Figure 15- Gas film formation time and gas film life time as a function of applied voltage in NaOH 30 wt.% [36]

2.9.Electrochemical Discharges

If the terminal voltage is higher than the critical voltage (typically about 25V), the growing bubbles coalesce and form an insulating gas film around the electrode. Hence, the electrolysis cease to occur and the current drops suddenly. Consequently, electrical discharges accompanied with light emissions occur across the gas film. Various terminologies are used in the literature: electrode effects, anode effects, electrochemical discharge phenomenon, and contact glow discharge electrolysis. In this thesis the term electrochemical discharge (ECD) is employed.

ECD has been known since the nineteenth century with the work of Fizeau and Foucault [36]. They were the first who observed light emissions during electrolysis and mentioned the analogy with the electrical discharges.

In 1889, two French scientists, Violle and Chassagny [53], studied the phenomenon quantitatively. They dipped two thin platinum electrodes into sulfuric acid 10%. They found that as they apply voltages higher than 32V, a gas film layer covers the thinner electrode and discharge takes place. They also observed that if the anode is the thinner electrode, terminal voltages that are higher than 50V must be applied in order to induce ECD.

During the 19th century, many studies were conducted to investigate the spectrum of the emitted light and the heat produced in ECD. It was found that the chemical composition of the gas formed around the thinner electrode (active electrode) is a mixture of hydrogen and components of electrolyte and electrode.

In 1894, Hoho and Lagrange [19] used the ECD process to harden aluminum. They employed an aluminum electrode as the cathode. They observed that an outer layer of the electrode is hardened while the inside remains unchanged. They also studied the effect of the voltage on the gas film formation. They found that at voltages higher than the water decomposition voltage and smaller than the critical voltage the normal electrolysis occurs. As the voltage is increased farther than the critical voltage, the electrolysis becomes unstable and some discharges happen. When the voltage is increased even further, the gas film becomes more stable.

In 1899, The German physicist, Wehnelt, observed [63] that the current is interrupted periodically during ECD. He used this effect in the first electrolyte interrupter, known as

the Wehnelt interrupter. Robert Bunsen was the first to observe the ECD effect in a molten salt electrolyte (during alumina electrolysis) [25]. The physics and fundamentals of electrical discharge through the gas film, described in the literatures, are presented in this chapter.

2.10. Nature of the Electrochemical Discharge

Electrical discharge consists of a current flowing through gases. There are three types of gas discharges [54]:

1. Townsend discharge
2. Glow discharge
3. Arc discharge

Typical current-voltage characteristics of gas discharges are shown in Figure 16. Townsend discharges occur when a free electron has enough energy to ionize a gas molecule. The produced electron may itself ionize another molecule. This process continues and an avalanche is formed. Low currents and high voltages are characteristics of the Townsend discharges. In glow discharges the electron production is due to heavy ion impacts.

During the arc discharges electrons are produced by thermo and (or) field emissions. Low voltages and high currents are characteristics of the arc discharge (See Figure 16).

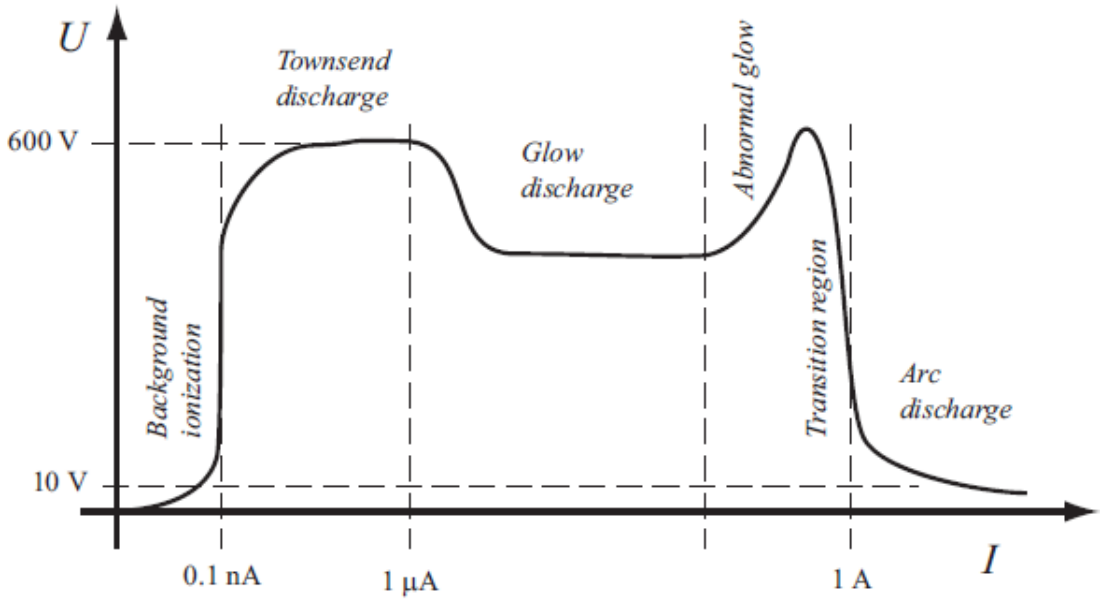

Figure 16- U-I characteristics of gas discharges [32]

Wüthrich [32] proposed that the electrical discharges happening in the electrochemical discharge phenomenon are thermo-initiated arc discharges. He mentioned the following reasons:

1. The characteristics (such as temperature, size and current density) of the discharges in the ECD process are all typical values of arc discharges.

2. The current-voltage characteristics of the ECD obey the Ayrton equation of arc discharges.

3. The temperature of the electrode is a few 100°C which is the temperature necessary for thermo initiation.

2.11. Current Signal during ECD

The current-time signal gives valuable information about the electrochemical discharges. The current signal can be used to determine the gas film formation time, the electrode surface, and the discharge activity [10].

The gas film formation time is the time required for the electrolyte to heat up. This time depends on the local temperature of the electrolyte. The gas film formation time may be representative of the temperature of the electrolyte [10]. Moreover, the magnitude of the current during the formation of the gas film represents the portion of the electrode length that is dipped into the electrolyte [32].

The discharge activity of the electrode can be monitored using the current signal obtained from the system. Figure 17 illustrates the current signal generated by an electrode in KOH 35 wt% solution. High values of the current (about 1 A/mm^2) show that no gas film exists. Current values of around 0.2-0.4 A/mm^2 indicate that the gas film is formed and discharges occur [37]. Furthermore, as mentioned in [32] discharges represent short pulses of a few 100 μs. Therefore, pulses of a few 100 μs with amplitude of around 0.2-0.4, in the current signal plot, correspond to discharges.

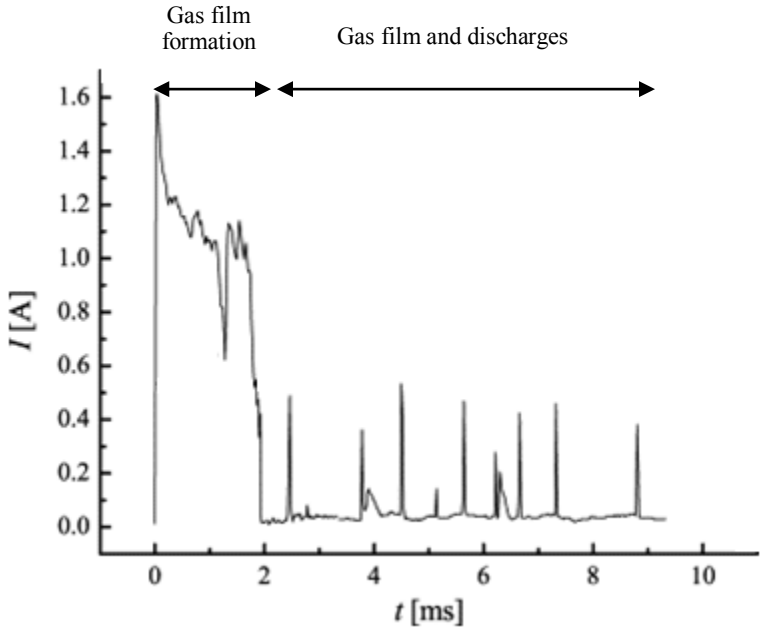

Figure 17- Current signal versus time at 50V for a 0.5mm diameter electrode in KOH 35 wt%

To describe the discharge activity, the probability of gas discharges per unit time and active surface area, λ_d, is introduced. λ_d, follows two different behaviors [38]. For the critical voltage increasing from U^{crit} to about $1.2U^{crit}$, λ_d decreases according to:

$$\boldsymbol{\lambda_d \propto -(U - U^{crit})^2} \tag{2.55}$$

and beyond $1.2U^{crit}$, λ_d increases with increasing applied voltage according to the following law:

$$\boldsymbol{\lambda_d = AE^2.exp\,(-\frac{B}{E})} \tag{2.56}$$

Figure 18 shows the probability of discharge as a function of applied voltage for NaOH 30 wt%.

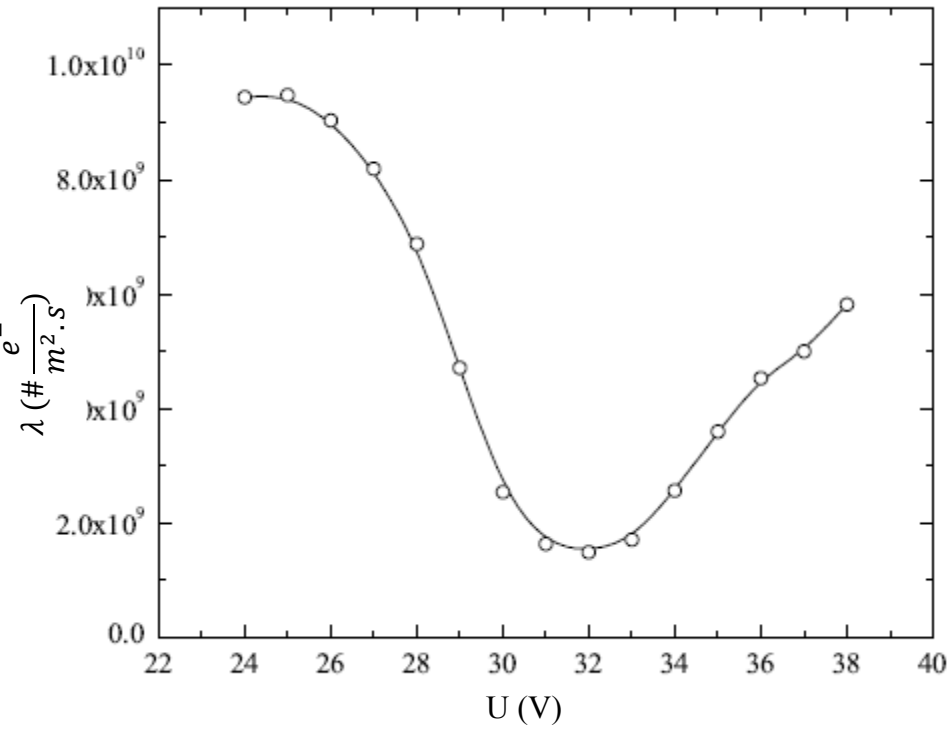

Figure 18- Probability of gas discharges in NaOH 30 wt% as a function of applied voltage [7]

The current signal also shows two different behaviors. In the first region, pulses of a few $100\mu s$ and $10\mu s$ are observed simultaneously. In the second region, only pulses of about $10\ \mu s$ are detected. The current signals for applied voltages of 25 V and 32 V are shown in Figure 19. This behavior is described by Wüthrich [7] as follows. For the region where λ_d is decreasing, the gas film covers only a part of the active electrode surface, and electrolysis takes place at the remaining parts. The current that is observed in this region may be the product of the combination of pulses from the electrolyte and pulses from the gas discharges. As the voltage increases, the gas film grows on the electrode until it blankets the electrode. From this point forward only arc discharges are detected.

a)

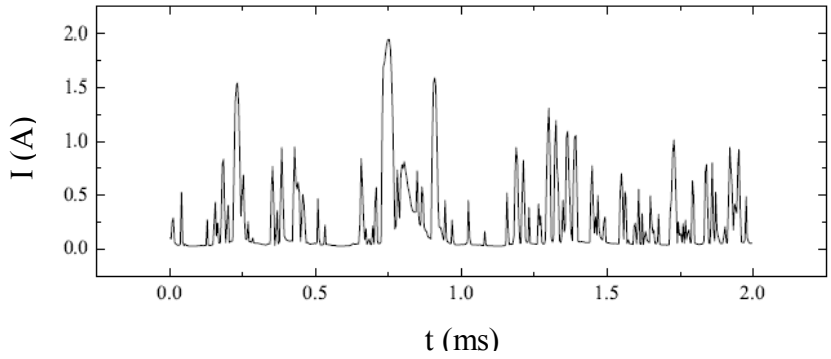

b)

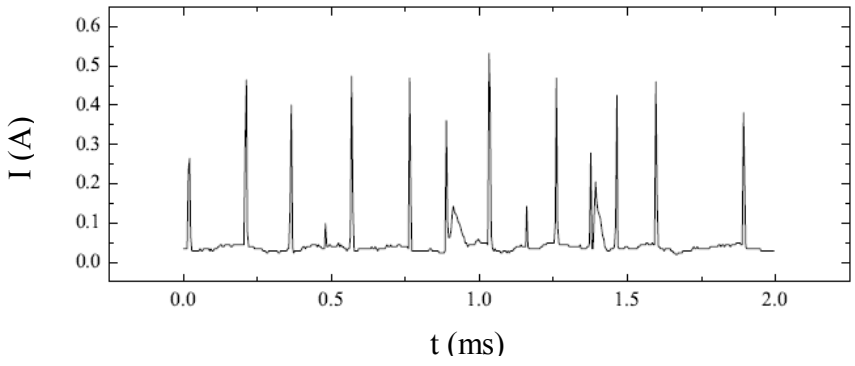

Figure 19- Typical current signal for applied voltage of a) 25 V and b) 32 V [7]

3. VISUAL OBSERVATIONS of ECD

Some characteristics information about the geometry and dynamic of gas film can be achieved by visual observation. In 1950 Kellogg [20] observed the gas evolution at the electrode. He used images to explain the anodic effect and compared the behavior of the gas evolving electrode at three different regions that he identified in his observations: Normal operation region, transition region, and anode effect region. In the normal operation region, bubbles evolve and leave the electrode. This region does not contain any noise. In the transition region, hissing noises arise and some of the gas bubbles are ejected downward. Condensed water vapor is observed indicating the high temperature of the electrode in this region. The hissing and ejection of bubbles stop at the anode effect region. A gas film blankets the electrode and a small spark is detected in the gas film. Kellogg used a camera with a 42-mm Micro-summer lens. The intensity of the light source was eleven times that of the sun and the duration of it was about 1/10000 second.

In 2005, Mena et al. [57] used image analysis to determine bubble size and shape in a bubble column. It was found that the most appropriate type of lighting for the effective observation of bubbles is the backlighting along with a diffuser screen between the camera and the bubble column.

Fascio [35], following her detailed description of the five phases of the current-voltage characteristics of a two-electrode cell as presented in chapter 2-4 of this thesis, proposed a model for the behavior of the current in each phase. She captured some images at each phase to support her model (Figure 20). She used a Nikon digital camera with exposure time of 1 ms and focal length of 2m. Fascio et.al [38] visualized the electrode to observe the gas film formation and the discharge activity.

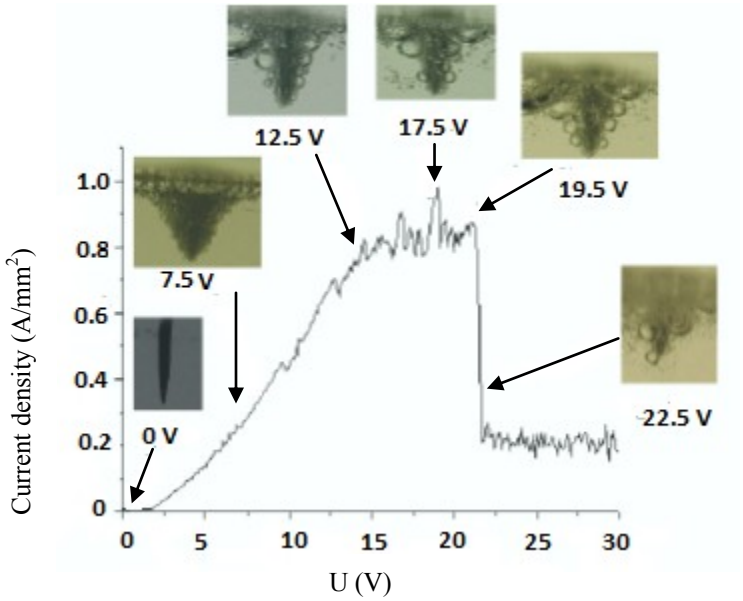

Figure 20- Typical current-voltage plot and corresponding behavior of the gas bubble at the working electrode [35]

The light emission from an electrode was investigated by observing the cathode [21]. For this purpose, a voltage cycle with a scan rate of 4.5 V/s was applied to a two-electrode cell. Three different regions, characterized with their type of discharges, were identified by referring to the images. Kazuhisa et al. [21] named the first region the permission region in which the hydrogen bubbles evolve. As the applied voltage increases, the temperature decreases and the glow discharges take place. The electrode surface emits a weak light in this region. At higher voltages, spark discharges are observed at the electrode surface. The Pt electrode melts during the spark discharges due to the high temperature. Furthermore, a glow discharge is not observed when the Pt electrode is employed as an anode.

In 1995, Raghuram et al. [39] investigated the effect of the circuit parameters on the electrochemical discharges by observing the behavior of the gas film. They studied the behavior of the current-voltage and the gas bubbles around the electrode for 4 different

voltages: Smooth DC, full wave rectified DC, smooth DC with a series inductor, full wave rectified DC with a serried inductor. It was observed that the drop in the level of current in the transition region is lower for the circuit containing an inductor. Moreover, discharges are intermittent for the circuit with inductor due to the back EMF.

In summary, the visual observations conducted so far were essentially of a qualitative nature and covered a limited range of parameters.

4.SOME APPLICATIONS OF ELECTROCHEMICAL DISCHARGES

ECD can be applied in different fields, such as surface engineering [1], waste water treatment [2], nano-particle production [3,4], micro machining of non-conductive materials [5,6,7], and reduction of metal salts.

4.1.Nanoparticles Synthesis Using Electrochemical Discharges

The fabrication of nano-particles is briefly reviewed by analyzing the synthesis process of nickel nano-particles. A nickel rod of 0.5mm diameter acting as the cathode and 20cm^2 of nickel acting as the anode are immersed in a sulfuric acid solution. By applying a cell terminal voltage of 32V, metal ions are produced and leave the anode due to the existence of the gas film. e_{aq}^- or H· radical contribute to the reduction of metal cation M^{z+} and the production of nano-particles. The following reactions show the process of the nano-particle production involving e_{aq}^- [40]:

$$H_2O \rightarrow e_{aq}^-, H., OH., H_2, H_2O_2, H_3O^+$$

$$e_{aq}^- + M^{z+} \rightarrow M^{(z-1)+}$$

$$e_{aq}^- + M^+ \rightarrow M^0$$

$$nM^0 \rightarrow M_2 \rightarrow \cdots \rightarrow M_n \rightarrow \cdots \rightarrow M_{agg}$$

Similarly, with the H· atoms:

$$H_2O \rightarrow e_{aq}^-, H., OH., H_2, H_2O_2, H_3O^+$$

$$H. + M^{z+} \rightarrow M^{(z-1)+} + H^+$$

$$H. + M^+ \rightarrow M^0 + H^+$$

$$nM^0 \rightarrow M_2 \rightarrow \cdots \rightarrow M_n \rightarrow \cdots \rightarrow M_{agg}$$

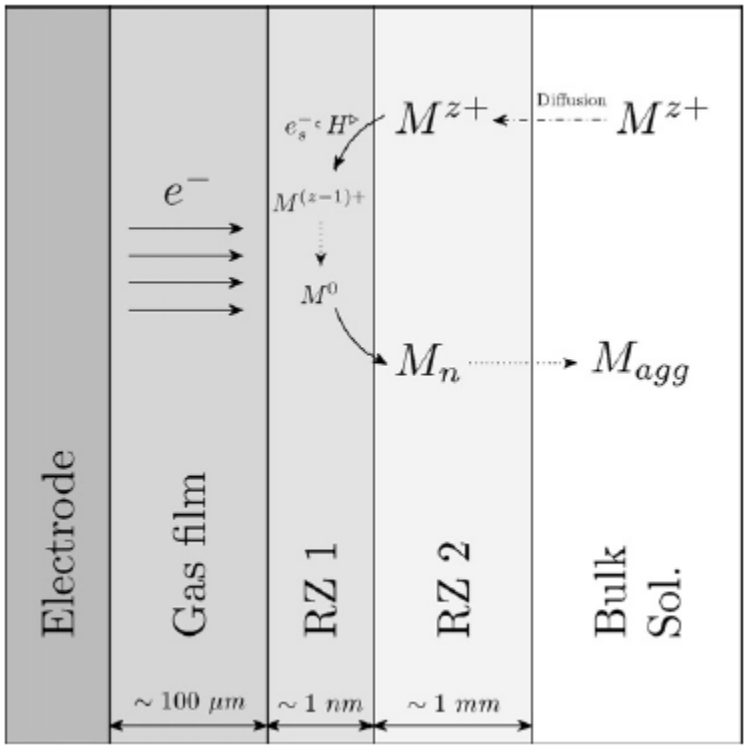

Figure 21-Reaction zones in electrochemical discharges [40]

The Ni nano-particles are obtained by pouring the solution containing nano-particles on an appropriate surface like a carbon mesh; after drying the mesh, the nano-particles remain. Also one can produce Ni nano-particles by adding Ni salts to the electrolyte.

It is believed [40] that there are other processes involved in the production of nano-particles, such as mechanical expulsion of nano-clusters from the cathode electrode and local melting of the cathode using high temperature discharges.

The synthesis of nano-particles using electrochemical discharges presents several advantages such as:

- Low cost
- Simplicity
- Great potential for industrial scale up

- Possibility to synthesize a large variety of metallic nano-particles

The most important advantage of this process is the low cost aspect. Chemical reactions, involving often expensive chemicals, are replaced by electrochemical reactions. For a given metal, the nano-particles, either in their bulk form of metal, or, what is often much cheaper, in its salts form, can be selected as precursor.

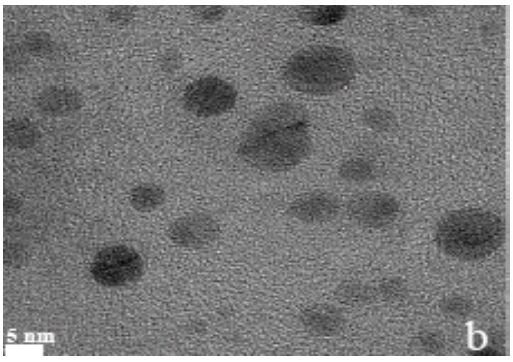

Figure 22- TEM micrograph of Nickel nano-particles synthesized by electrochemical discharges [40]

4.2.Micro-Machining Using Electrochemical Discharges

Non-conductive materials such as ceramic and glass have been of great interest in modern industry. Ceramics are characterized by their light weight, improved strength, low thermal expansion coefficient and corrosion resistance, and glass is distinguished by its chemical resistance, biocompatibility and transparency. However, the main limitation in using these materials is the structuring process. In effect, machining of these materials is not possible using traditional methods.

Several types of material processing like chemical etching, photo-forming, ultrasonic machining, powder blasting and laser machining, and machining with diamond tools are used. The limitations of these techniques include cost, machining time, and machining surface quality. Spark Assisted Chemical Engraving (SACE) is a viable alternative for these techniques.

Machining glass can be accomplished using a diamond tool. The limitation of this method is the cost of machining, since the diamond is expensive and is worn easily [42] Moreover, the 3D micro-structuring is not possible with such method [32]. Furthermore, laser machining is expensive. The surface quality is often not acceptable [32]. Ultrasonic machining can be used for cutting, grinding and finishing but the material removal rate in drilling is low [42]. Chemical etching and photo-forming have slow machining rates. Machining of high aspect ratio structures is difficult using this method [32].

The erosive effect resulting from the discharges was first observed by Joseph Priestly [46] in 1770. SACE was proposed in 1968 by Kurafuji [5]. Several names are given to SACE such as chemical discharge machining [30], spark assisted etching [43], electrical discharge drilling [5] or electrochemical spark machining [44]. The term SACE was first used by Langen et al. in [45].

SACE is a cheap process as the cost of the equipments involved is low. The tools used in SACE are inexpensive either; they may be manufactured of stainless steel. An additional interesting feature of SACE is its flexibility. The SACE tool electrode does not come into contact with the sample, therefore vibration, chatter and mechanical stresses are eliminated [46] .A mechanical prototype is designed by Langen et al.[45] to use SACE machining. No active control has been reported so far, however, several passive control strategies are developed recently by Wüthrich [32].

Although the process of SACE has not been mastered completely yet, however, the basic fundamentals of this procedure are described. During ECD, if the sample is located at a distance less than $25\mu m$ [47] from the electrode then the machining process is possible. A schematic of the experimental setup is shown in Figure 23.

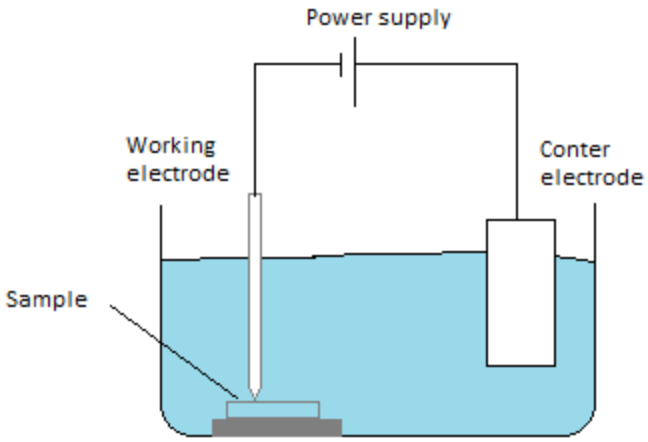

Figure 23- Experimental set up for SACE machining

Yonghong et al. introduced a new type of ECD machining, gas-filled electro-discharge and electrochemical compound machining in [42]. They filled the area surrounding the electrode with a particular gas using a gas-filled system to allow the electrical discharges to take place. This replaces the gas film formed by the electrochemical reactions. Such method, however, is not efficient for holes with a depth higher than 1.5mm and a diameter greater than 2mm.

There are some limitations for this procedure. In fact, the gas film created around the electrode is not stable and the machined surface may be damaged because of the occurrence of micro-explosions. The local temperature increases as well which may result in cracks on the surface of the sample [32].

4.3.Surface Engineering Using Electrochemical Discharges

ECD can be applied for surface modification and coating. Lazarenko et al. [1] used discharges for heat treatment of the surface. There are other applications of this phenomenon in surface engineering, such as cleaning, etching and polishing. Surface

coating using this particular technique yields a surface with wear, friction, corrosion and thermal properties mainly required in aerospace applications, textile and gas and oil industries. [1].

There exists a wide range of setup in this application depending on the purpose of the application. It is obvious that the choice of electrode material and electrolyte is different when the setup is required for cleaning surfaces and surface coating. In the anodic configuration, oxidation may result in corrosion or oxide based coating of the surface depending on the type and chemical composition of the solution [1].

One of the advantages of this technique is its flexibility. When coating using the ECD technique, the morphology and crystal structure of the coating layer is possible by changing the applied voltage and temperature [48].

As an example, the work conducted by Paulmier e al. [49], which consisted in the deposition of diamond-like carbon, is described in the present section. A cathodic configuration (cathode is smaller than anode) in a two-electrode cell is used. The electrolyte is composed of ethanol, water, potassium chloride and phosphate buffer. By applying a voltage, oxygen bubbles form around the working electrode (cathode). Then, by increasing the voltage, a gas film covers the electrode and ECD happens. The analysis of the components of the solution [49] shows that different chemical processes occur during ECD. Nano-crystalline graphite and oxide components are generated as a result of ECD. The surface is prepared for deposition using the thermal effect of ECD. Ionized species in the plasma are propelled toward the surface and implemented on the surface.

5. EXPERIMENTAL SETUP

5.1. Materials

- NaOH and KOH were purchased from Fischer Scientist. They were used as received and no further purification was performed.
- 0.5 mm diameter Nickel rod at 99.98% purity and 5×5 cm^2 Nickle sheet at 99.98% purity were purchased from Alfa Aesar.
- Clear cast acrylic sheets with 3mm thickness were purchased from McMaster-Carr.
- Deionised (DI) water

5.2. Set Up

- Figure 1 shows a layout of the experimental setup. A conventional two-electrode electrochemical cell that is 10cm long and 10cm width and of 5cm height was used. The cell was made of a clear cast acrylic sheet that provides a clear view of the electrode. The cathode, active electrode, was a Nickel rod, and the anode, counter electrode, was a nickel sheet. Typically, the active electrode has a much smaller surface area than the counter electrode (in the order of 1/100). The active electrode was attached to a holder in such a way that it can move vertically to adjust the immersion depth into the solution.
- The DC power supply used was the ZUP60-3.5 model from TDK Lambda. A function generator, 33220A model from Agilent, was used to apply a pulsed voltage. The maximum output voltage from this function generator is 10 V_{pp}. An

amplifier from AVTECH was employed to increase the voltage output of the function generator.

- Current signals were collected by an Agilent current probe model N2774A-50 MHz which was connected to an Agilent DSO 3102A-100 MHz digital oscilloscope.
- A Phantom V 9.1 camera was used to observe the working electrode.
- The software used to control the camera and analyze the images was a Phantom camera control V660-0-0.
- Videos from the camera were collected by a desktop computer.
- 3 LED lamps were used to illuminate the electrode. Two lamps were located on both sides of the cell at a distance of 10cm. One lamp was installed on top of the camera to illuminate the electrode from the front.
- A pulse coming from the function generator was used to synchronize the camera and the oscilloscope. A transistor was used to adjust the voltage output from the power supply to the voltage required by the camera to be triggered

5.3.Experiment

The work was carried out by the study of the current signals and video images.

- The electrolyte solutions were prepared by dissolving NaOH or KOH in DI water. 300 mg DI water was placed in a plastic bottle. Depending on the concentration, NaOH or KOH was measured and added to the water. A concentration of 10 %, 20 % and 30 % wt NaOH and 7%, 15% and 35% wt. KOH were used. NaOH and

KOH are exothermic materials, therefore, they must be added slowly to the water and the liquid must be swirled while preparing the solution.

- Observation of the electrode and analysis of the flow around it were conducted using a high resolution high speed camera. The depth of the focus was optimized such as to achieve clear visualization of the bubbles and the gas film around the electrode. The sample rate was set to 1000 frames per second to allow visualization of the gas film formation. Exposure time was $997\mu s$. Image capture was triggered by the signal coming from the function generator. The quality of the recorded video images was improved using the Phantom camera software. Each video was converted to PNG images using MATLAB software.
- The electrode diameter was used to calibrate the size scale. Three random images were selected, and the gas film thickness was measured at six different locations on each image. It was not possible to determine directly the gas film thickness from the images. The electrode diameter was subtracted from the gas film diameter and then divided by two.
- The gas film formation time was measured by counting the number of images from t = 0 to the time at which the gas film was formed. The time interval between the two images was set to1 ms.
- The velocity of the gas film was measured by displacement of the gas film waves over the time interval. For each solution, the average velocity of four different waves was considered as the velocity of the gas film.
- The experiments were performed at room pressure and temperature.

6. RESULTS AND DISCUSSION

6.1. I-U Characteristics of the System

The voltage scan technique is employed in the present research to better understand the ECD phenomenon. This technique consists in applying a triangular shaped voltage (Figure 24), then measuring the current response and coupling it with the photographs of the electrode.

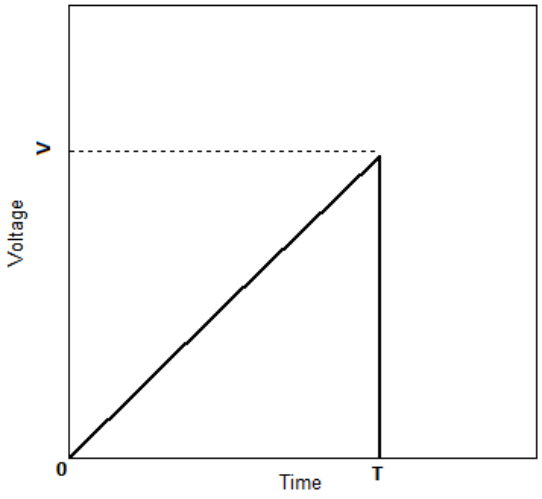

Figure 24- A triangular shaped voltage applied to a two-electrode cell

As discussed in section 2.5, the mean stationary I-U characteristics can be separated into five different regions [18,20]: thermodynamic region, ohmic region, limiting current region, instability region and arc region. Based on the observations, the arc region is further divided into two regions: invisible arc region and visible arc region. Figure 25 presents a plot of the current as a function of the voltage for KOH 35 wt.% at $25°C$. The plot is obtained from the average of ten voltage scans between 0 to 45V with a scan rate of 45 V/s. The numbers on the graph indicate the different regions. The behavior of the

bubbles and the flow around the electrode in each region is described next. In Figure 27, the typical time-series of the current density and the corresponding images are reported. The nominal current density $\frac{I}{A}$, where the electrode surface area, A, is calculated based on the images (Figure 26.a).

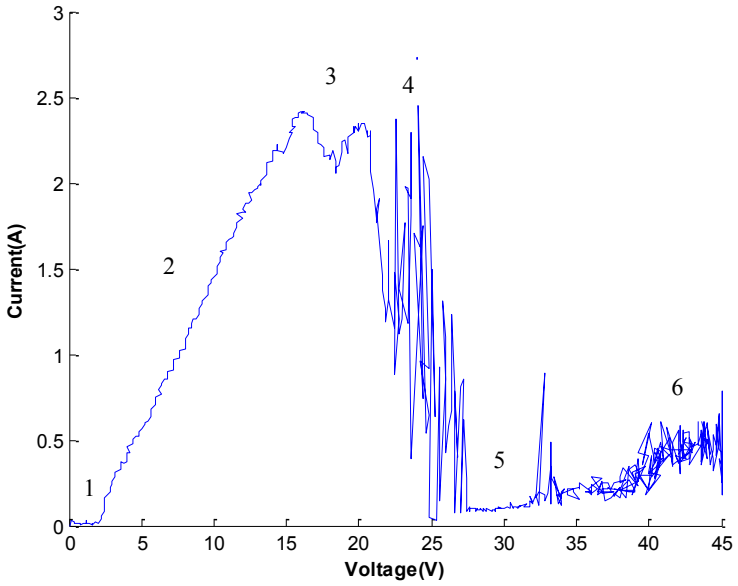

Figure 25 – Average current signal obtained from ten voltage scans between 0 to 45 at a rate of 45 V/s. and illustration of six different regimes (See text for explanation). The electrode is a 0.5mm diameter Ni rod and the electrolyte KOH 35%.

For each region, described in section 2.5, a sequence of images are taken and analyzed. The cell terminal voltage V is set to a voltage belonging to a region in the I-U characteristics of KOH 35% as shown in Figure 25. A 100 ms step input of voltage V is applied to the setup comprised of a 0.5mm diameter nickel as the working electrode, a nickel sheet is used as the counter electrolyte and KOH 35 wt% as the electrolyte. The cell terminal voltage is used as well to trigger the camera and the oscilloscope that collects the current signal. Image analysis is employed to study each region by direct observation of the electrode.

$0 < V < 2.2$: *thermodynamic and over-potential region*; in this region no electrolysis happens and no bubble is observed around the electrode.

$2.2 < V < 14$: *ohmic region*; this region is initiated when the applied voltage exceeds the water decomposition voltage U_d. The electrolysis of water takes place and bubbles form at the nucleation sites on the electrode surface. When a bubble leaves the surface of the electrode, another one forms in its nucleation site. Bubbles leave the electrode surface, move upward and accumulate at the electrolyte-air interface. They create a conical envelope around the electrode. All the bubbles around the electrode have almost the same diameter (about 150 μm), except the ones located outside the envelope which have a larger diameter (about 350 μm) . The volume of this conical envelop does not change with time. Figure 26.I depicts the current signal and images of an electrode at 10V. The signal follows an exponential trend. This behavior is explained later in section 4.2.

$14 < V < 22$: *limiting current region*; the number of active nucleation sites increases with increasing current density. Therefore, more bubbles form on the electrode surface. In this limiting region, the number of active nucleation sites reaches its maximum. This region can hence be characterized by the coalescence of bubbles and turbulent flow. Furthermore, increasing the voltage increases the size of the bubbles. Figure 27 presents the growing bubbles after 3ms at 10V and 20V in KOH 35 wt%. As mentioned previously in section 2.5, the coalescence critical time is dependent on the size of the growing bubbles. In fact, increasing the size of the bubbles decreases the coalescence critical time and hence the bubbles coalesce at a smaller contact time. When the applied voltage is 20V, the bubbles are much larger than those produced at 10V. Consequently, the coalescence critical time is smaller. This indicates that at 10V, the coalescence time is

greater than the contact time whereas at 20V, the opposite is true. This means that at 20V, the contact time is enough for the bubbles to coalesce.

$22 < V < 25$: *instability region*; in the instability region (or transition region) a gas film is formed around the electrode. However, as shown in the images, the system is highly unstable and may be sometimes in the limiting region. This instability can also be seen in the current signal. Figure 26.III presents the current signal and the corresponding images at 23V. Two different behaviors are observed around the electrode:

1- Turbulent flow similarly to the limiting region.

2- Gas film formation

$25 < V < 35$: *invisible arc region*; a thin stable gas film covers the electrode. This region has not been mentioned in the literature. It was believed that when the gas film forms, discharges occur between the electrode and the electrolyte. However, it is observed that a gas film can be present for a long time without or with only a few discharges occurring. Although the discharges are not present in the images, peaks in the current signal indicate their existence. This region is therefore called the invisible arc region. Figure 26.IV exhibits the current signal and the corresponding images of KOH 35 wt% at 30V. This region is also observed for NaOH 30 wt%.

$35 < V$: *visible arc region*; the temperature of the electrode is high enough to induce thermo-initiated arc discharges [7]. As a result, sparks accompanied with light emissions are observed. At lower voltages, the sparking takes place at the tip of the electrode (Figure 26.V). As the voltage is increased, the sparks begin to take place all over the surface of the electrode and their number increases.

I.

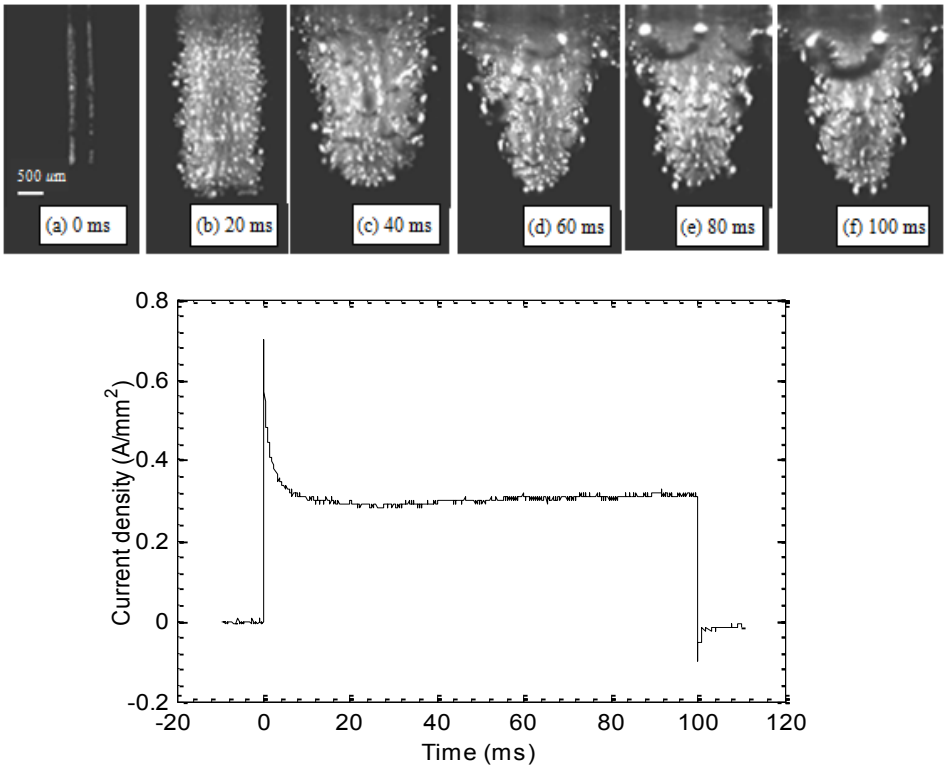
500 μm
(a) 0 ms
(b) 20 ms
(c) 40 ms
(d) 60 ms
(e) 80 ms
(f) 100 ms
Current density (A/mm^2)
0.8
0.6
0.4
0.2
0
-0.2
-20
0
20
40
60
80
100
120
Time (ms)

II.

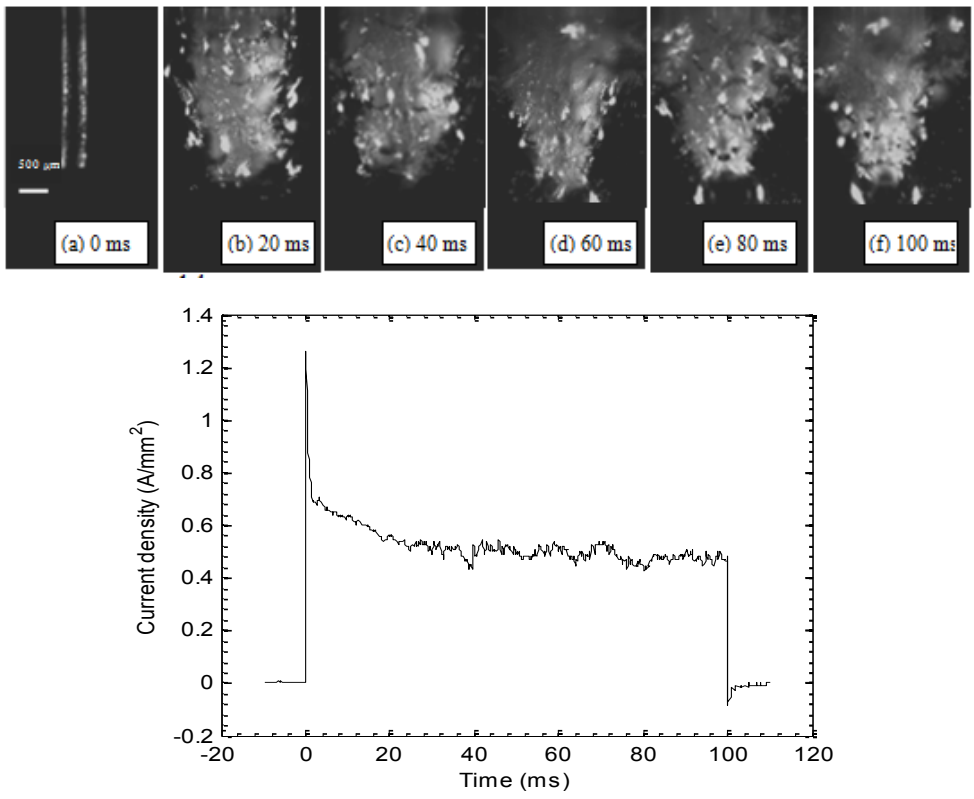
500 μm
(a) 0 ms
(b) 20 ms
(c) 40 ms
(d) 60 ms
(e) 80 ms
(f) 100 ms
Current density (A/mm^2)
1.4
1.2
1
0.8
0.6
0.4
0.2
0
-0.2
-20
0
20
40
60
80
100
120
Time (ms)

III.

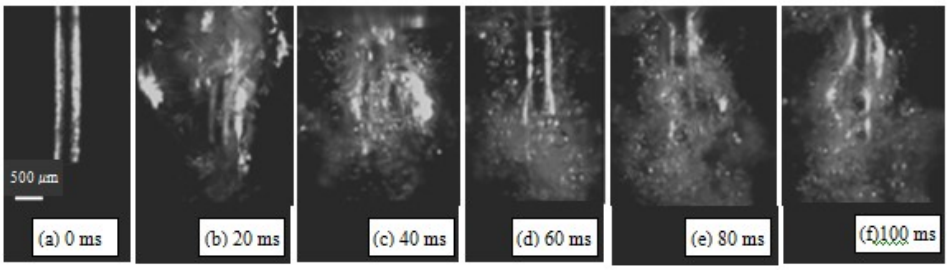
500 μm
(a) 0 ms
(b) 20 ms
(c) 40 ms
(d) 60 ms
(e) 80 ms
(f)100 ms

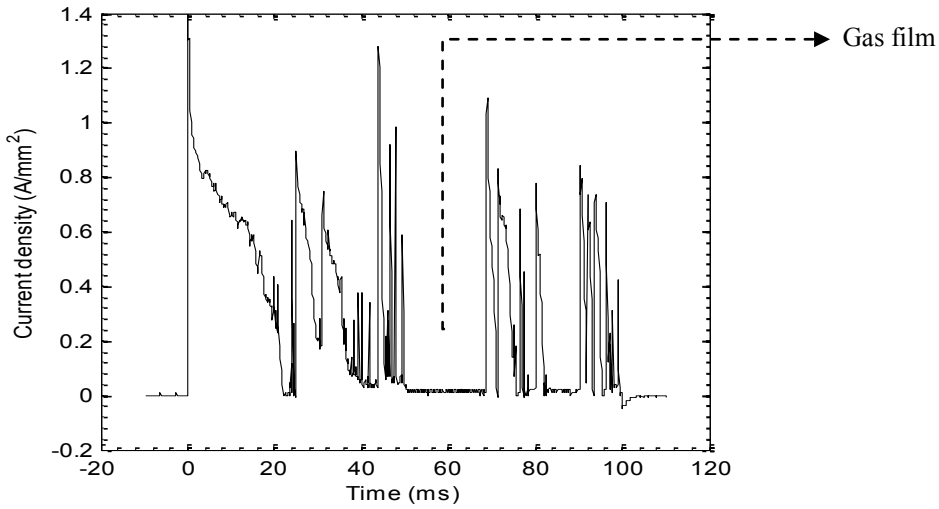
Current density (A/mm2)
Time (ms)
Gas film

IV.

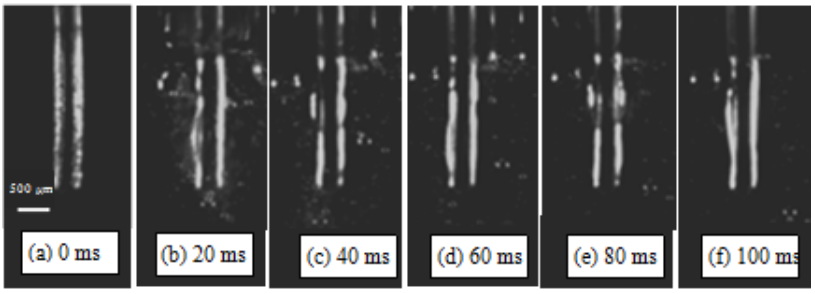
500 μm
(a) 0 ms
(b) 20 ms
(c) 40 ms
(d) 60 ms
(e) 80 ms
(f) 100 ms

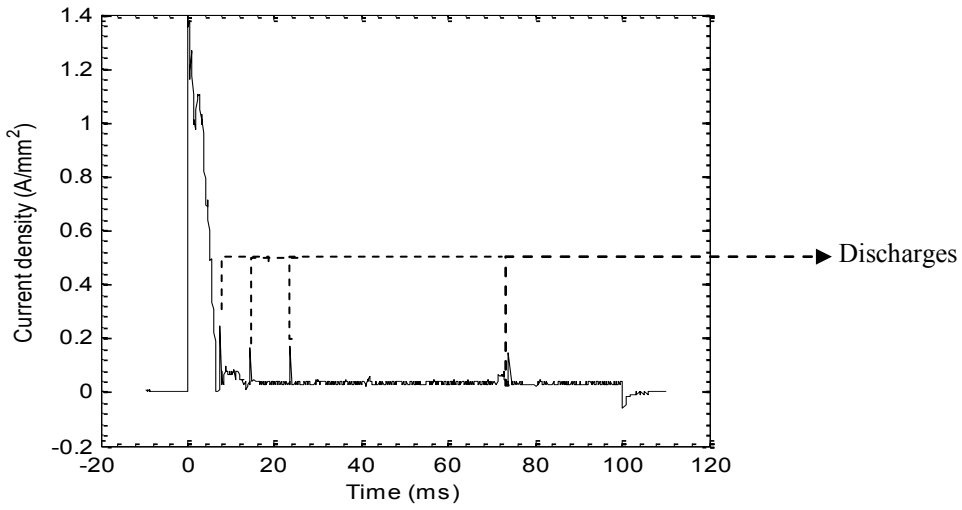
Current density (A/mm2)
Time (ms)
Discharges

V.

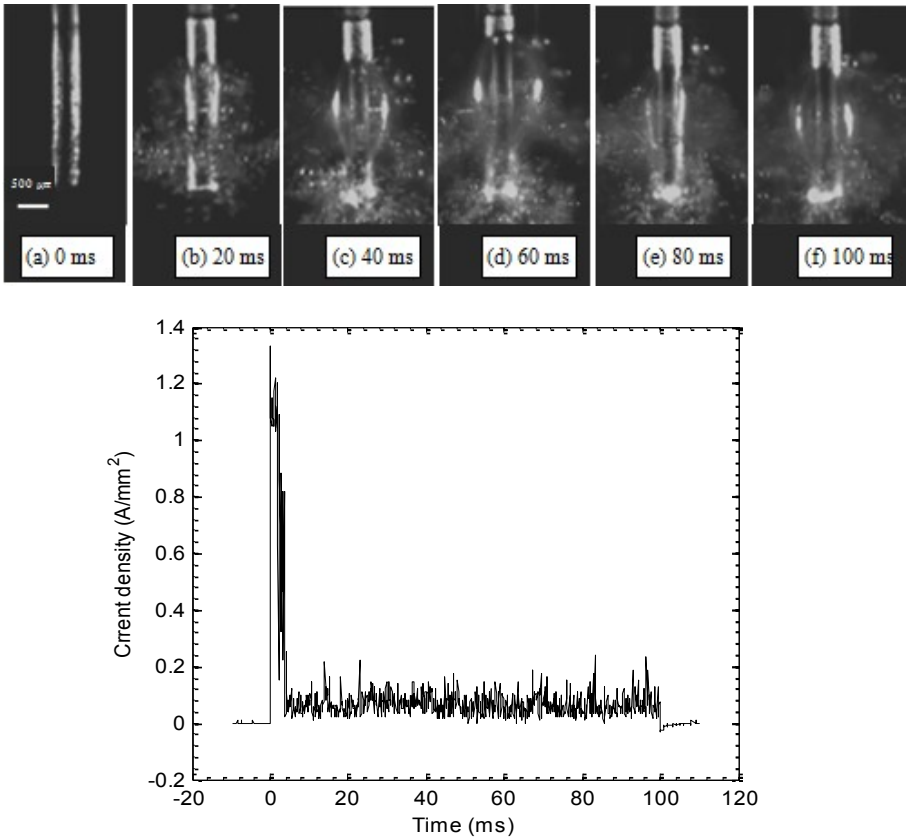

Figure 26- Current signal and video images for KOH 35 wt%, the electrode is a 0.5mm diameter nickel rod dipped in 3mm of electrolyte, the applied voltage is a step input of I)10 V II) 20V III) 23V IV) 30V V) 40V

a) b)

Figure 27-Comparison of the bubble size around the electrode in KOH 35 wt%, a) 10V, b) 20V, growing bubbles are larger at 20V

6.2.Bubble Formation

In the engineering applications of ECD, there is a great interest in understanding the evolution of bubbles around the electrode or in other word the characteristics of the system prior to the formation of the gas film. The behavior of the system before the gas film formation is investigated in the present section.

6.2.1. The resistance of the electrolyte

As mentioned in section 2.3, the formation of the bubbles increases the inter-electrode resistance. The inter-electrode resistance before and after the formation of the bubbles as well as the bubble coverage fraction is experimentally measured.

Figure 28 shows a typical current time-series at a step input of a voltage lower than the critical voltage. I_o is the initial current, when the bubbles are not formed yet (see Figure 26.I.a). I_∞ is the current at the end of the step input, when the bubbles are around the electrode (see Figure 26.I.f).

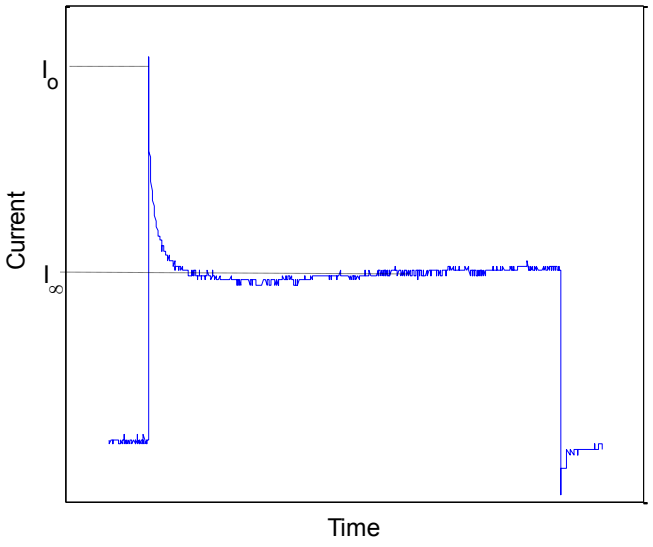

Figure 28- Typical current-timeseries at a voltage lower than a critical voltage. I_o is the initial current and I_∞ is the current when bubbles are formed at the electrode

The resistance of the electrolyte, prior to the formation of bubbles, is measured using the I_o-U graph. Since, no bubble is present at I_o , the slope of the graph represents the conductivity (1/resistance) of the electrolyte. Figure 29, shows the change in the initial current, I_o in the function of the cell terminal voltage. As expected, the current increases linearly as the voltage increases. The reason the current fluctuates at the end of the graph is that the system reaches the power limit of the used power supply. By measuring the slope of this graph, one can find the resistance of the electrolyte R_o, which in the case of KOH 35% is about 3.33Ω.

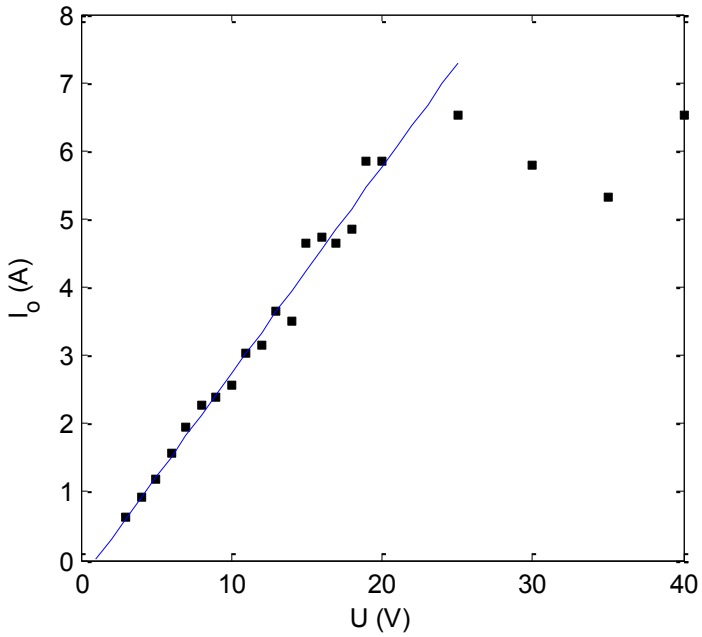

Figure 29- The initial current I_0 in function of cell terminal voltage. The electrolyte was KOH 35% and the electrode was a 0.5 mm diameter nickel dipped 3mm in electrolyte.

The increase in the resistance due to the formation of bubbles can be estimated using equation 2.29. The bubbles form a random close packing structure. The volume void fraction for a random close packing of sphere is about 0.36 ($\varepsilon = 0.36$). The radius r and the length h of the electrode are 0.25mm and 3mm, respectively. The thickness of the

bubble layer, d, for KOH 35% is found to be 0.375mm, using Figure 30. The conductivity of KOH 35% is 0.65 s/cm. Substituting these values in the equation 2.29 yields 1.4Ω for the resistance of the bubble layer (R_{diff}).

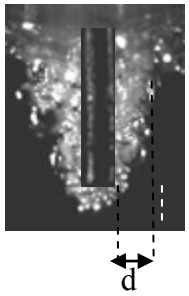

Figure 30- Bubble layer around an electrode. d is the thickness of the bubble layer.

Note that in the equation 2.29, the shadowing of the surface by bubbles is not considered. By increasing the bubble coverage fraction θ the resistance of the bubble layer increases. This equation can be modified as:

$$\boldsymbol{R = \frac{R_{diff}}{1-\theta}}\,[7] \tag{6.1}$$

The total resistance of the system after the formation of bubbles is

$$\boldsymbol{R_{\infty} = R_o + \frac{R_{diff}}{1-\theta}} \tag{6.2}$$

Considering equation 6.2, one can find the bubble coverage fraction θ as

$$\boldsymbol{\theta = 1 - \frac{R_{diff}}{R_{\infty} - R_o}} \tag{6.3}$$

In the above equation, R_{diff} can be found using equation 2.29, R_o using the I-U graph, as described earlier and R_{∞}can be found using

$$\boldsymbol{\frac{I_o}{I_{\infty}} = \frac{R_{\infty}}{R_o}} \tag{6.4}$$

As an example, the bubble coverage fraction at three different voltages is given in Table 1. As can be seen, the resistance of the electrolyte as well as the bubble coverage fraction increases with increasing cell terminal voltage. As mentioned previously, when the voltage increases, more nucleation sites are activated and hence more bubbles are formed. The formation of bubbles increases the inter-electrode resistance.

Table 1- Summary of the process of finding the bubble coverage fraction in KOH 35%

Voltage (V)	I_o(A)	I_∞(A)	$\frac{I_o}{I_\infty} = \frac{R_\infty}{R_o}$	R_∞(Ω)	θ
10	2.56	1.32	1.9	6.27	0.54
15	4.64	2.08	2.2	7.26	0.65
20	5.84	2	2.9	9.57	0.77

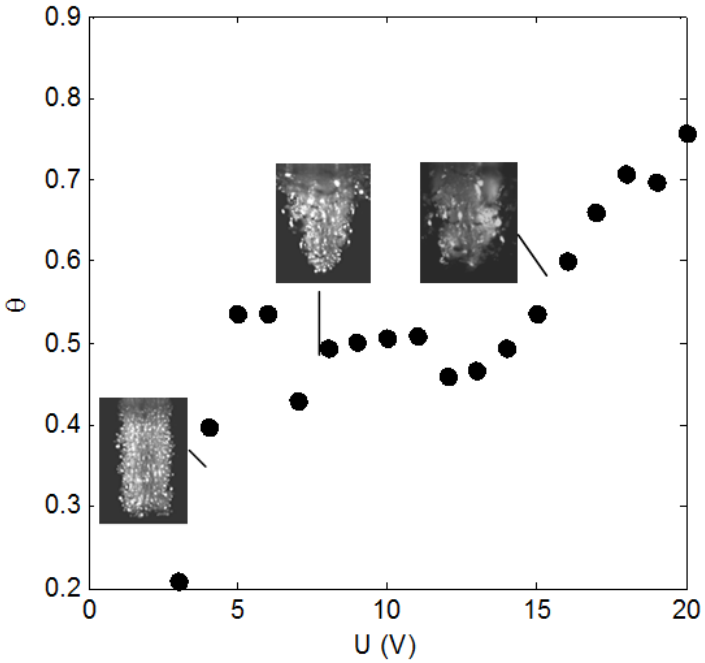

Figure 31- The bubble coverage fraction in function of the cell terminal voltage for a 0.5 mm diameter and 3mm length electrode in KOH 35%

The bubble coverage fraction in function of the cell terminal voltage is shown in Figure 31. By increasing the voltage more nucleation sites are activated. Therefore, the rate of

bubble production and consequently the bubble coverage fraction increases. At a certain voltage (5V for KOH 35%) the bubble layer forms a conical shape and by increasing voltage (up to 15V) it keeps the same shape. As it can be seen from the graph in this range the bubble coverage fraction remains constant. By increasing the cell voltage, over 15V, the bubble coverage fraction increases until it reaches to its maximum and the gas film forms.

6.2.2. Normalized current

The normalized characteristics are of great interest in the theoretical and practical analysis of a system. The normalized current and voltage as defined by Wüthrich [7,32] describes the behavior of the system independently of the electrode and electrolyte properties. The experimental data is used to validate the model introduced by Wüthrich [7,32].

The current time-series can be described as well in a form that is independent of the electrode geometry and the electrolyte properties as mentioned in [7]. The normalized current is defined as:

$$\bar{I} = \frac{I}{I^{crit}} \tag{6.5}$$

The normalized current time-series obtained with a 0.5mm diameter Nickel rod electrode in KOH 35% for a step input of 10V and 20V is shown in Figure 32. The solid line is the normalized current predicted according to equation 2.53. This equation yields the current through the electrode before the formation of the gas film. The critical voltage, U^{crit}, critical current I^{crit}, and water decomposition potential U_d were measured from the mean I-U plot of KOH 35% (Figure 25). The voltage at which the instability region begins (the

current drops suddenly) is the critical voltage and the corresponding current is the critical current. U^{crit} is determined to be 22V, the water decomposition potential U_d is 2.2V, and the critical current I^{crit} is 2.4A The results obtained with equation 2.53 agree well with the experimental data for the percolation threshold of 0.5 (Figure 32).

a) U = 10V, $\overline{U}$ = 0.35

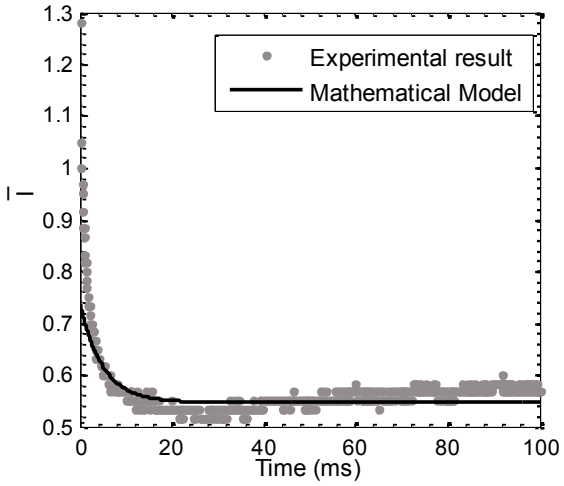

b) U = 20V, $\overline{U}$ = 0.85

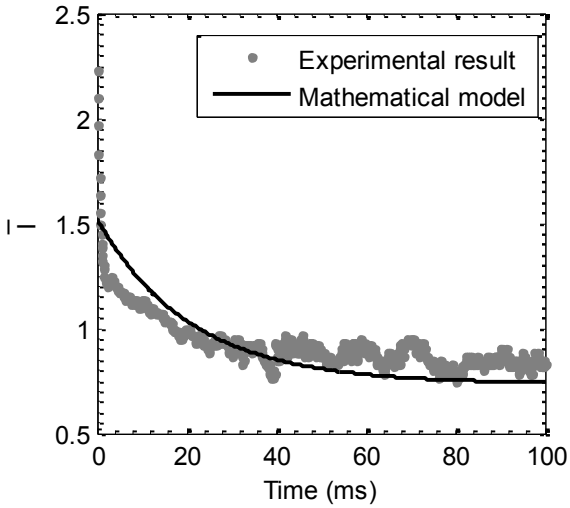

Figure 32- Comparison between the predicted normalized current timeseries using the percolation method (equation 2.53) and the experimental measurements at a) 10Vand b) 20V. U^{crit} , U_d, $I^{crit}$and θ_c are 22V, 2.2V, 2.4A and 0.5 respectively.

6.3.Gas Film Formation

6.3.1. Gas film formation time

In this section, the effect of the cell terminal voltage on the gas film formation time is investigated. The current signal is recorded for each solution at voltages ranging from 25 to 60V. A 100 ms step input of voltage V is applied to the setup described in section 3. The electrolytes that were employed are NaOH with the concentration of wt.10%, wt.20% and wt .30 and KOH with the concentration of wt. 7%, wt. 15% and wt. 35%. The gas film formation time, t_f, is estimated for each case, based on the obtained current signals, as shown in Figure 33. The change in the gas film formation time with respect to the voltage is illustrated in Figure 34. As observed in Figure 34, the cell terminal voltage presents a significant impact on the gas film formation time. In effect, the gas film formation time decreases asymptotically with increasing voltage.

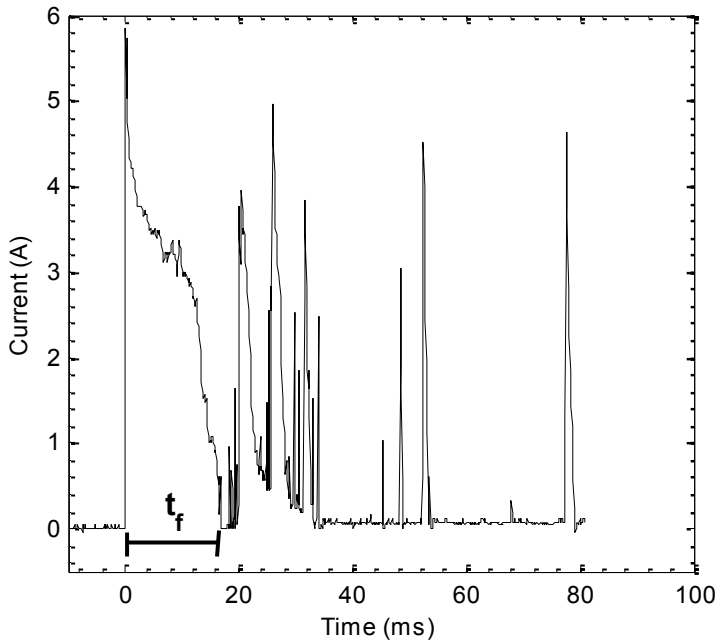

Figure 33- A typical current timeseries of ECD in 30 wt% NaOH solution at 25V. One pulse with a period of 100ms is applied. The active electrode is a 0.5mm diameter Nickel rod dipped in 3mm of an electrolyte solution. The gas film is formed after a time t_f= 18ms.

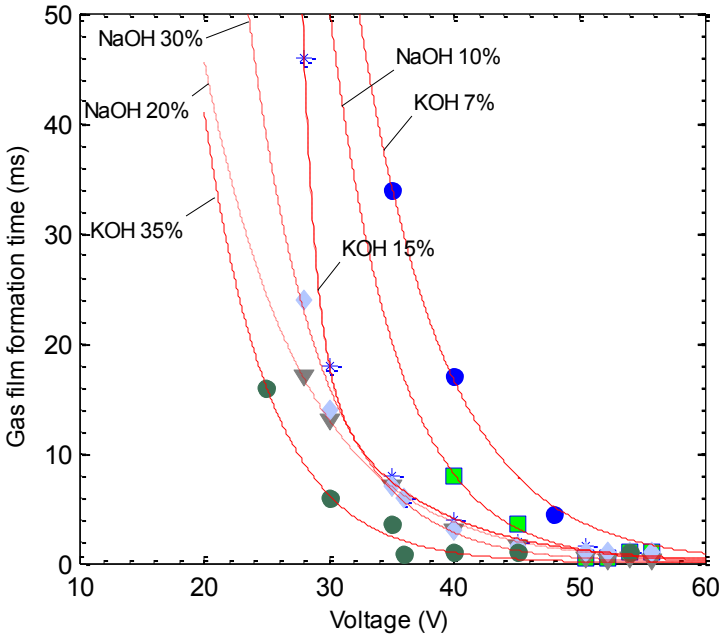

Figure 34- Gas film formation time vs. applied voltage. Results obtained with six different solutions are presented.

The voltage can be expressed in a form independent of the electrode geometry and the electrolyte properties. The normalized voltage is defined as:

$$\bar{U} = \frac{U - U_d}{U^{crit} - U_d} \tag{6.6}$$

Figure 34 shows that the gas film formation time is strongly dependent on the electrolyte. It is difficult to determine a relation between t_f and the electrolyte properties. However, Figure 35 indicates that the gas film formation time can be described using the normalized $\bar{U}$.

The critical voltage, U^{crit}, for the experimental configuration used in the present study, for each solution, is estimated from the mean I-U characteristics and is tabulated in Table 2. The water decomposition potential, U_d, is obtained experimentally and its value was found to be 2.7.

The gas film formation time can be estimated using Equation 2.55. This equation fits well with the experimental measurements for the percolation threshold, θ_c=0.5 and the bubble detachment time, $\Delta t_b = 8.6\, ms$ (Figure 35). This validates the model developed [7] by Wüthrich based on the percolation theory. This model considers the electrochemical gas evolution as a mechanism involved in the gas film formation.

Table 2- The critical voltage of six different solutions for the used experimental configuration

Solution	NaOH 10%	NaOH 20%	NaOH 30%	KOH 7%	KOH 15%	KOH 35%
Critical voltage (V)	29	26	25	35	26	22

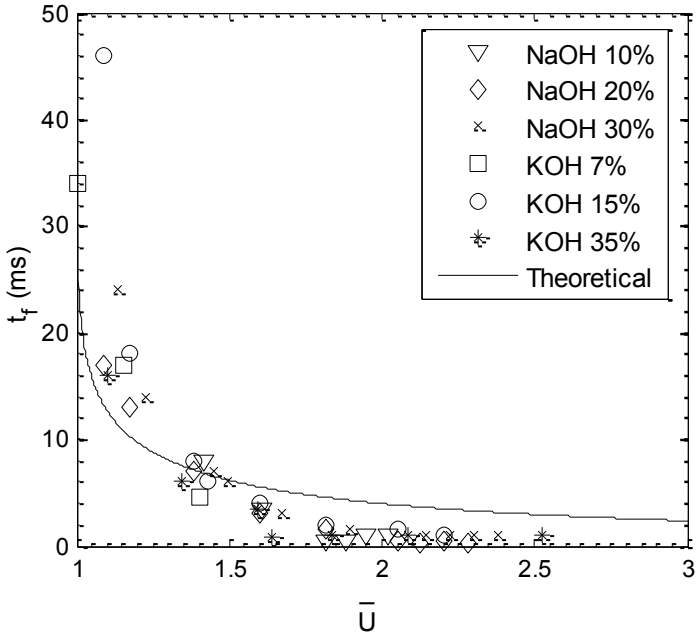

Figure 35- Gas film formation time for six different solutions vs. normalized U. The solid line is plotted according to equation 2.55 for the percolation threshold of 0.5.

In this model the time is normalized as:

$$\frac{t_f}{\Delta t_b} \tag{6.7}$$

However, Figure 35 is a normalized graph representing t_f as a function of the normalized voltage $\bar{U}$. This implies that Δt_b is a constant value for the electrolytes and the experimental condition used in this study.

Klupthy estimated as well the change in the gas film formation time with the cell terminal voltage. In his model, equation 2.30, Klupthy considered that the change in the gas film formation time is due to the evaporation of the electrolyte by the local joule heating.

Figure 36 shows the experimental results and the estimated gas film formation time using the thermal model developed by Klupthy. As shown in the figure, this model does not explain the experimental results. Comparing Figure 35 and Figure 36 indicates that for the configuration used in the present study, the percolation model provides a better prediction model of the gas film formation time.

Table 3- Solution properties at room temperature [58,59,60]

Solution	NaOH 10%	NaOH 20%	NaOH 30%	KOH 7%	KOH 15%	KOH 35%
Density (kg/m^3)	1098	1210	1333	1068	1145	1337
Surface tension (mN/m) $\times 10^{-2}$	8.184	8.877	9.655	7.906	8.348	9.776
Electrical conductivity (S/m)	30	32	20	15	45	65
Specific heat (J/kg.K)	3782.5	3627.5	3535.5	3717	3378	2880
Evaporation temperature (K)	475	481	490	474	477	492

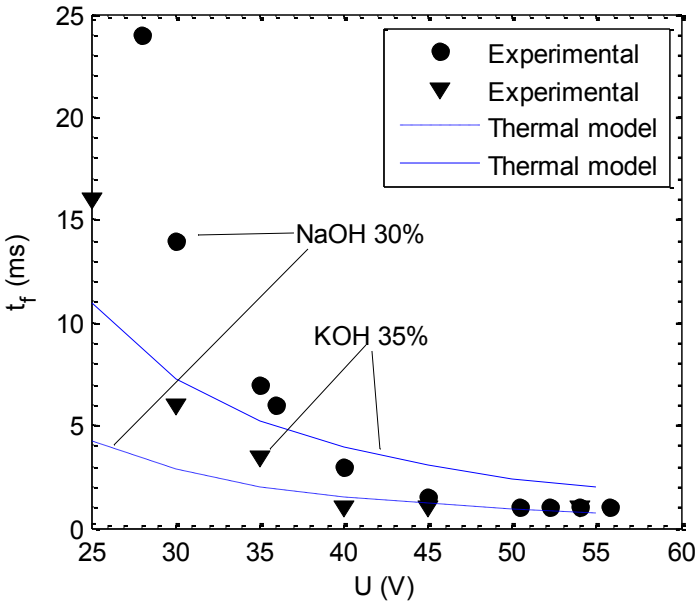

Figure 36- Gas film formation time in function of the cell terminal voltage. Comparison of the experimental results and the model developed based on the local joule heating using $U_d = 2.7$, $T_o = 25℃$, $R = 3.3Ω$ and the electrolyte properties shown in .Table 3.

6.3.2. Gas film thickness

The gas film thickness significantly affects the quality of discharges [10]. In order to study the gas film thickness, voltages in a range from 20V to 50V is applied to the cell. Figure 37 shows the gas film thickness in four different solutions as a function of the cell terminal voltage.

The variation in the film thickness can be described by Figure 38. Sometimes a very thin gas film lies on the electrode surface (Figure 38-a and b) and sometimes a bubble shape forms at some places (Figure 38-c). As a result the mean gas film thickness increases.

To compare the gas film thickness in different solutions, it is measured at the invisible arc region for KOH 7 wt.%, 15 wt.%, 35 wt.% and NaOH 10 wt.%, 20 wt.% and 30 wt.%. Discharges are not visible in the invisible arc region (see Figure 26.IV). This allows measuring the gas film thickness based on the images captured. From the mean stationary

I-U characteristic, a voltage corresponding to the invisible arc region is selected. The selected voltages are tabulated in Table 4. Since the gas film is not uniform, it is measured at three different points on the electrode surface using six different images. Then, the average of all values is considered as the gas film thickness. The reported thickness for the gas film for a typical cylindrical electrode with a diameter of 1mm is 50-100 μm and a few millimeters in [20]. The gas film thickness that was determined in the present study ranges between 50 to 100 μm (Table 4). The reported variation in the parameters is primarily due to measurement errors.

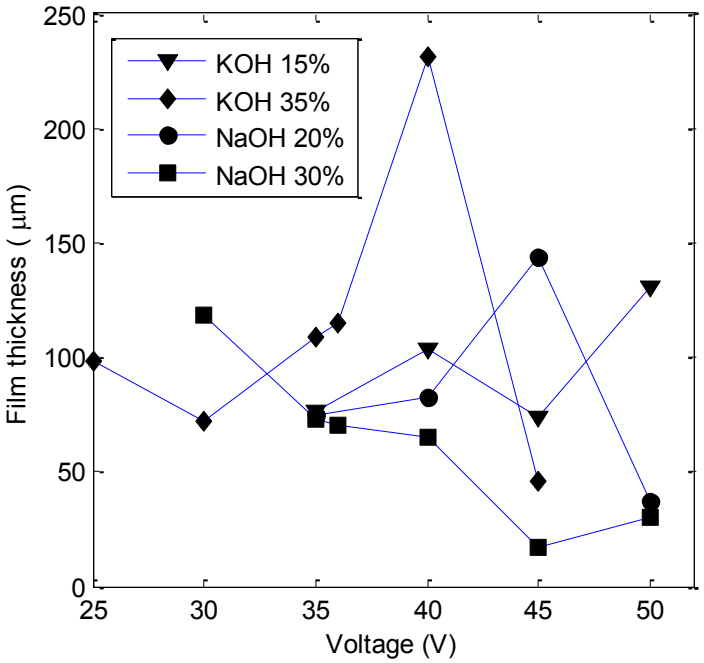

Figure 37- Gas film thickness in different solutions in function of the cell terminal voltage with a cylindrical electrode of 0.5 mm diameter and the length of 3mm.

In [10] the film thickness, d_f, is evaluated using

$$b\frac{\pi}{2}\xi d_n = (b + d_f)^2 - b^2 \tag{6.1}$$

where b is the electrode radius and ξd_n is the mean bubble diameter. Some typical results are listed in Table 5. Comparing Table 4 and Table 5 indicates that equation 6.8 overestimates the value of the film thickness.

a) b) c) d)

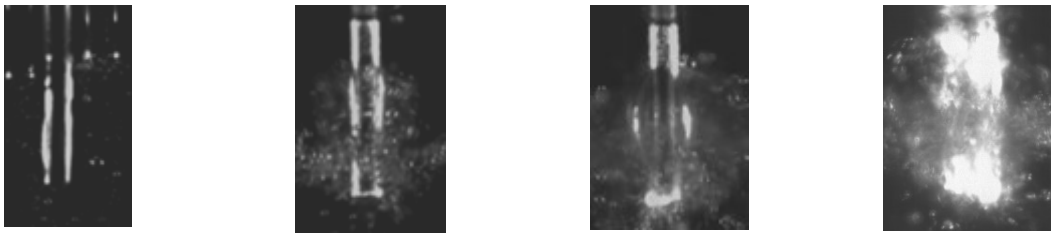

Figure 38- Different configurations of the gas film

Table 4- Measured gas film thickness based on the images at the selected voltages

Solution	NaOH 10%	NaOH 20%	NaOH 30%	KOH 7%	KOH 15%	KOH 35%
Selected voltage (V)	40	35	35	40	35	30
Gas film thickness (μm)	83±2	74±2	70±2	84±2	76±2	72±2

Table 5- Estimated gas film thickness using equation 6.8[10]

Solution	NaOH 10%	NaOH 20%	NaOH 30%
Gas film thickness (μm)	220	103	172

6.4.Hydrodynamic Effects on a Gas Film

Understanding the hydrodynamic effects on the gas film is important since the hydrodynamic forces define the shape and the thickness of the gas film. In the present section, the effects of the hydrodynamic parameters on a gas film are investigated. The Weber and Reynolds numbers are identified as two important dimensionless parameters, based on the Pi theorem and dimensional analysis, in the study of the gas film formation.

The Pi theorem is used to analyze fluid mechanic problems. It states that "If an equation involving k variables is dimensionally homogeneous, it can be reduced to a relationship among k-r independent dimensionless products, where r is the minimum number of reference dimensions required to describe the variables [50]."

According to the Pi theorem, any meaningful equation with k variables denoted by u_i, such as

$$\boldsymbol{f(u_1, u_2, \dots, u_k) = 0} \tag{6.2}$$

can be re-written as

$$\boldsymbol{\phi(\Pi_1, \Pi_2, \Pi_3, \dots, \Pi_{k-r}) = 0} \tag{6.3}$$

where Π_i are dimensionless terms (Pi terms) and are independent of each other. These terms are composed using the variables u_i. The number of Pi terms required to define a system is k-r, where r is the minimum number of reference dimensions. Therefore, the number of variables in a fluid mechanics problem is reduced from k to k-r.

Several variables u_i are selectively recurrent in all Pi terms. In effect, the number of repeating variables equals to the number of the reference dimensions. These repeating variables are combined with the remaining variables to create a Pi term. All of the reference dimensions must be included in the repeating variables. Furthermore, the dimensions of each repeating variable cannot be a combination of the dimensions of other variables.

The variables that are involved in the present problem consist of the length L, density ρ, viscosity μ, velocity V and surface tension σ. In terms of the basic dimensions (reference dimensions), they are expressed as $[L]$, $[ML^{-3}]$, $[ML^{-1}T^{-1}]$, $[LT^{-1}]$ and $[MT^{-2}]$ respectively. The density ρ, viscosity μ are the properties of hydrogen (the fluid inside

the gas film) which are shown in Table 6. Surface tension σ is the property of the interface of the solution and air (shown in Table 3). L is considered as the mean thickness of the gas film which is shown in Table 4. The velocity of the gas in the gas film is considered as velocity V.

Table 6- Properties of air at room temperature

Density ρ (kg/m^3)	0.08376
Dynamic Viscosity μ (N.s/m^2)	8.909×10^{-6}

The Froude number

$$\boldsymbol{Fr} = \frac{\boldsymbol{V}}{\boldsymbol{C}} \tag{6.4}$$

is the ratio of inertia force to the weight of a fluid. It is an important dimensionless number in the problems involving with the free surface and represents the velocity of the fluid to the velocity of the waves on the fluid surface. Froude number is assumed to be equal one. Therefore, the gas velocity will be the same as the velocity of the waves.

The velocity of the gas is estimated by measuring the velocity of the wave peaks (see Figure 39). The waves move along the electrode. The distance that each peak wave travels over a period of time gives the velocity of each wave. The average of all wave peaks velocities yields the velocity of the gas film. The estimated velocities of six different solutions are shown in Table 7.

Figure 39- Gas film waves of a 0.5mm diameter electrode, dipped in 3mm of NaOH 30%. Characteristic velocity is estimated using the average of the velocity of the wave peaks.

Table 7- Estimated gas film velocity in each solution

Solution	NaOH 10%	NaOH 20%	NaOH 30%	KOH 7%	KOH 15%	KOH 35%
Gas film velocity (μm/s)	139±2	126±2	136±2	169±2	175±2	149±2

Since there are five variables ($k = 5$) and three basic dimensions ($r = 3$), the required number of Pi terms, based on the Pi theorem, is equal to two. The length L, density ρ and velocity V are selected as repeating variables seen that the dimensions of these variables are independent. As mentioned previously, the dimensions of each variable cannot be produced by the combination of the dimensions of the other variables. The repeating variables are combined with the non-repeating variables μ and σ to form non dimensional terms. The two Pi terms that are created are the Weber and Reynolds numbers:

$$\boldsymbol{We = \frac{\rho V^2 L}{\sigma}} \tag{6.5}$$

$$\boldsymbol{Re = \frac{\rho V L}{\mu}} \tag{6.6}$$

Finally, the result of the dimensional analysis can be expressed as:

$$\frac{\rho V^2 L}{\sigma} = \phi\left(\frac{\rho V L}{\mu}\right) \tag{6.7}$$

This indicates that the current problem can be investigated using these two dimensionless terms.

The Reynolds number is a dimensionless parameter that represents a measure of the ratio of the inertial forces to the viscous forces. The Reynolds numbers that are calculated in the present problem are smaller than 1 (Figure 40) which indicates that the viscous forces are dominant.

The Weber number is an important dimensionless number for the analysis of fluid flow problems that present an interface between two different fluids. It is a measure of the ratio of the inertial force to the surface tension force. This number is useful in the study of thin film flows and the formation of bubbles and droplets.

The form of the function ϕ can be derived from the experimental data. As shown in Figure 40, there exists a linear relationship between Reynolds and Weber number.

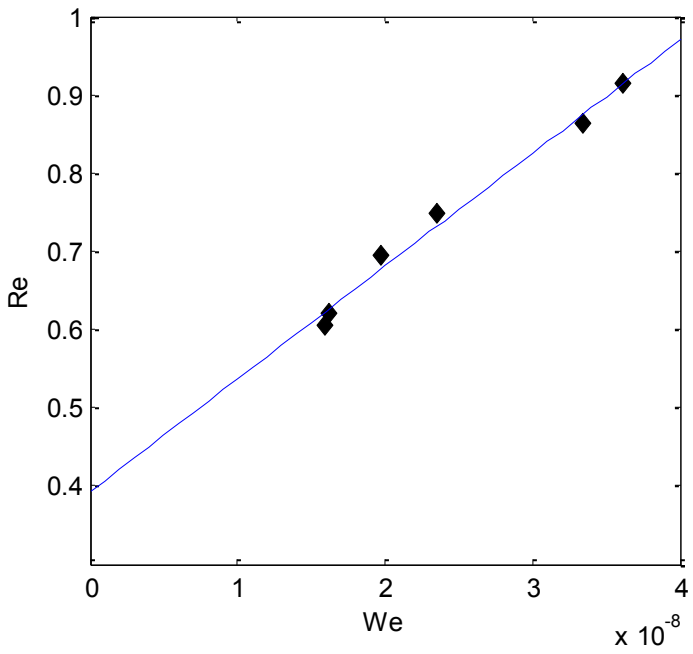

Figure 40- Weber number vs. Re number

6.5.Controlling ECD

In the previous sections, the parameters influencing the gas film were investigated to allow a better control of the ECD. The current section aims to determine experimentally, a way to control the gas film. Since the gas film is the medium required for arc discharges, its quality significantly impacts the various applications of ECD. For example, in machining applications, the unstable gas film induces fluctuations in the electrochemical discharges and leads to a low repeatability of the machining process, therefore deteriorating the machining quality [10].In nanoparticle production using ECD an unstable gas film results in unstable discharges and, consequently, inhomogeneous nanoparticles. The purpose of the present work is to derive a way to control the gas film. Based on visual observations, it is found that the combination of the partially covered electrode and offset pulsed voltage yields a stable gas film and consequently stable discharges.

The electrode is partially covered with a glass (Figure 41.a). A partially covered electrode exhibits a different behavior from a conventional electrode. A spherical gas film (a large bubble) forms around the covered electrode rather than a cylindrical one (Figure 41.c). This observation is in agreement with the finding in [51].

A bubble forms around the electrode when a voltage is applied to a covered electrode. The bubble grows until it reaches a maximum diameter and then breaks. As soon as it breaks, another bubble forms there, grows and breaks. This cycle repeats as long as a cell terminal voltage is applied.

A different gas film shape indicates a different behaviour in the discharges. When the new growing bubble is still small (the film is thin enough), a discharge is observed at the

tip of the electrode (Figure 41.d). However, as the bubble becomes larger the discharge is no longer possible.

The lifetimes of the different growing bubbles are equal. This implies that the time intervals between two discharges are equal. Thus, a regular discharge is achieved by covering the electrode.

Not only discharges occur regularly by covering the electrode, but also undesirable discharges are prevented and the ECD is localized. Nevertheless, discharges are not continuous (they occur periodically) which decreases the efficiency of the ECD. It is possible to induce continuous discharges with a covered electrode by applying an offset pulsed voltage.

Applying a pulsed voltage consists of interrupting the current and the supply of the gas products. This prevents the bubble from growing during the off-time of the voltage (Figure 42). Hence, the gas film bursts before it transforms into a large bubble. However, the gas film and the discharges remain unstable since the gas film breaks and forms.

To overcome this problem a small constant voltage (offset) is applied during the off-time (Figure 43). Recently, the offset pulse voltage is used to improve machining with electrochemical discharges [52]. Applying the offset voltage prevents the gas film from bursting during the off-time; however, as the current is still not strong enough, the gas film cannot grow and form a large bubble. Therefore, a stable gas film with continuous discharges is created (Figure 43).

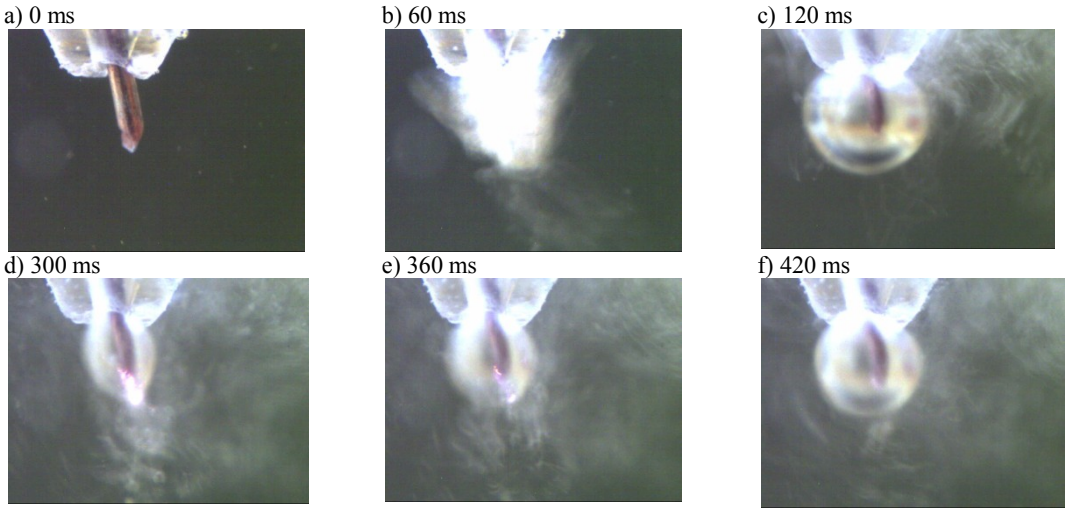

Figure 41- A series of images of a partially covered electrode. A large bubble forms around the electrode rather than a gas film. The electrode is a 0.5 mm diameter Nickel rod covered with glass

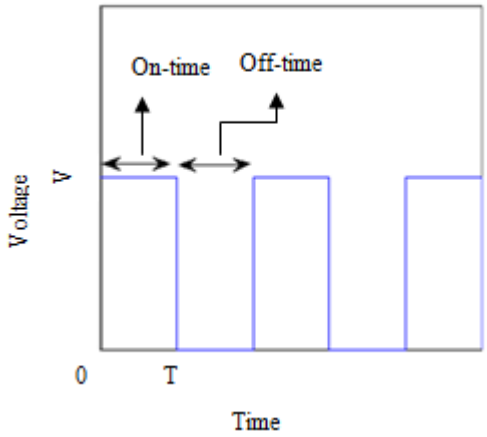

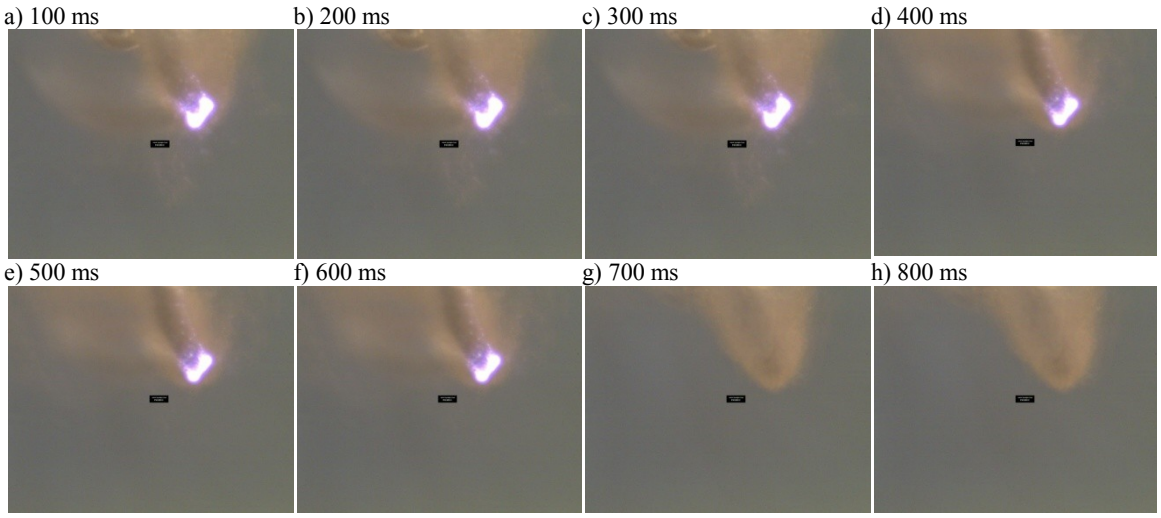

Figure 42- Pulsed voltage applied to a covered electrode (top), a gas film forms during on-time and breaks during off-time before transforming into a large bubble, on-time: 200 ms off-time:600ms at 50V(bottom)

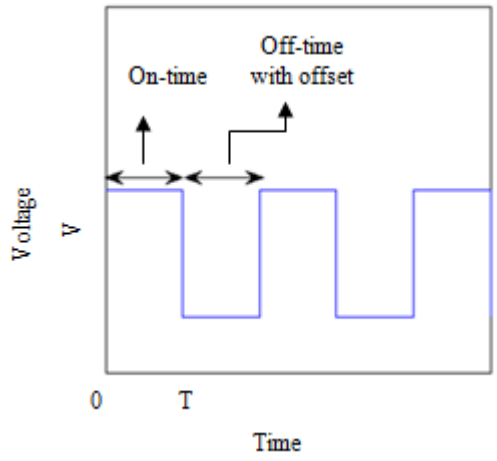

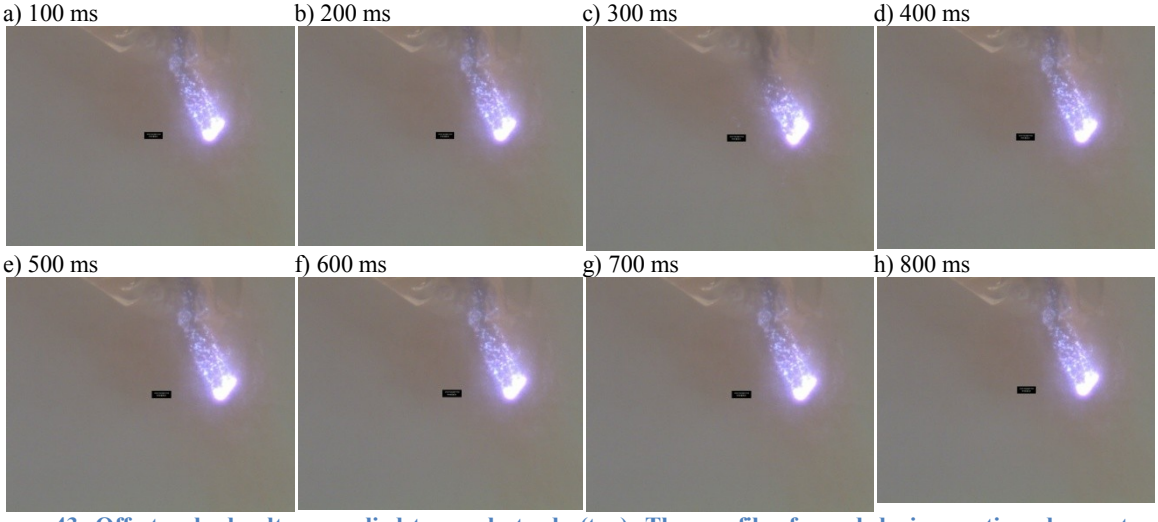

Figure 43- Offset pulsed voltage applied to an electrode (top). The gas film formed during on-time does not break during off-time because of the offset voltage, however, the current is too small and the gas products are not enough to form a large bubble. On-time: 10 ms, off-time: 10ms at 50v, offset: 12V (bottom)

7.CONCLUSION

The gas film properties as well as the factor affecting these properties are studied. Moreover, to better understand the ECD phenomenon the behavior of the system prior to the formation of the gas film is investigated. The contributions of the present study are explained in the following section. Then, the possible applications are discussed and some suggestions for future works are provided.

7.1.Conclusions

The following conclusions can be drawn from the present study:

- The experimental data that was obtained in the present study validates the model developed by Wüthrich. The latter is characterized by the fact that the electrode effect is modeled based on the percolation theory. The experimental data confirms that the normalized current and voltage introduced by Wüthrich define the behavior of the system independently of the electrolyte properties and the electrode geometry.
- The I-U characteristics plot is interpreted through the images of the electrode that were captured during the experiment. There exists an extra region in addition to the five that are mentioned by other researchers. In this region, the gas film is present for a long period of time without (or with a few) discharges.
- The coalescence of the bubbles in the limiting current region is attributed to their large size. As the current increases the bubble size increases. Consequently, the critical coalescence time decreases and becomes smaller than the contact time. Therefore, the rate of coalescence grows by increasing the voltage.

- ECD is controlled using a covered electrode and applying an offset pulsed voltage.
- The Weber and Reynolds numbers are two important dimensionless parameters that are employed in the analysis of gas film formation. There exists a linear relation between the Weber and the Reynolds numbers of the gas film.

7.2.Discussion and Future works

A number of problems need to be solved for further development and improvement of the ECD applications. Based on the results obtained in the present thesis, the following recommendations are made for future works:

- Using a covered electrode and simultaneously applying an offset pulsed voltage may improve the surface quality of machining with SACE (Spark Assisted Chemical Engraving) technique. Covering the electrode prevents the undesired discharges from occurring on the electrode surface. The offset pulse voltage combined with a covered electrode results in stable discharges. This method can be applied as well in nanoparticle production with ECD. Since the discharges are stable, the nanoparticles produced are homogenous. However, the effectiveness of the proposed methodology needs to be experimentally verified.
- Decreasing the gas film thickness yields a higher reproducibility of the machining with SACE [10]. The Weber and Reynolds numbers define the shape and the thickness of the gas film. This implies that the film thickness can be modified by varying Reynolds and Weber numbers. However, further investigation is required to determine the quality of the effect of these parameters on the gas film.

- A thinner gas film can also be obtained if the critical voltage decreases [10]. The size of the bubbles is determined to be an effective factor in coalescing bubbles during the ECD process and the critical conditions are reached as the bubbles coalesce. If the bubbles coalesce at lower voltages the critical voltage is lower as well. Therefore, the possibility of modifying the bubble size requires further investigations. Moreover, additional parameters, such as the change in the concentration of the electrolyte at the electrode-electrolyte interface, which may affect the coalescence of the bubbles, need to be further examined.
- It is observed in the arc region that there exists a difference between the current signals for KOH 35 wt% and that for NaOH 30wt% (Figure 44). The high current signal depicted for the case of NaOH 30% indicates that there are more discharges when the solution is NaOH 30. Further work is required to identify the causes of the difference in the discharge behavior for the different solutions.

a) KOH 35 wt%

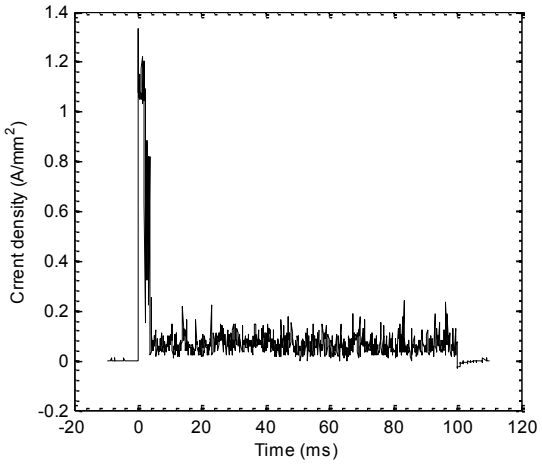

b) NaOH 30%

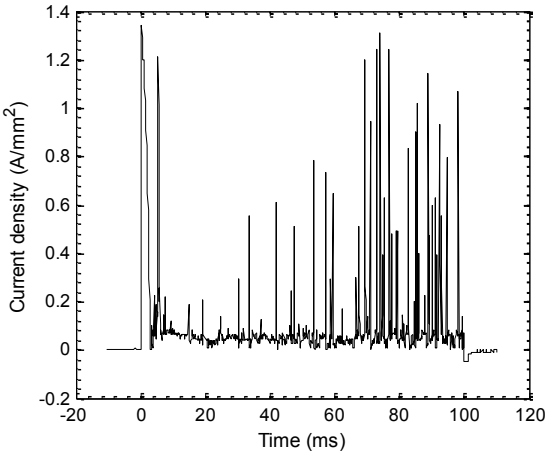

Figure 44- Comparison of the current signal at 40V a) KOH 35% and b) NaOH 30%. The electrode is a 0.5 mm diameter nickel rod dipped 3mm in the electrolyte.

REFERENCES

[1] Yerokhin, A. L., Nie, X., Leyland, A., Matthews, A., & Dowey, S. J. (1999). Plasma electrolysis for surface engineering. *Surface and Coatings Technology, 122*(2-3), 73-93.

[2] Jin-zhang, G., Xiao-yan, W., Zhong-ai, H., Jing-guo, H., & Quan, L. (2001). A review on chemical effects in aqueous solution induced by plasma with glow discharge. *Plasma Science and Technology, 3*(3) 765.

[3] Kawamura, H., Moritani, K., & Ito, Y. (1998). Discharge electrolysis in molten chloride: Formation of fine silver particles. *Plasmas & Ions, 1*(1), 29-36.

[4] Lal, A., Bleuler, H., & Wüthrich, R. (2008). Fabrication of metallic nanoparticles by electrochemical discharges. *Electrochemistry Communications, 10*(3), 488-491.

[5] Kurafuji, H., & Suda, K. (1968). Electrical discharge drilling of glass. *CIRP Annals, 16*(1), 415-419.

[6] Wüthrich, R., & Fascio, V. (2005). Machining of non-conducting materials using electrochemical discharge phenomenon—an overview. *International Journal of Machine Tools and Manufacture, 45*(9), 1095-1108.

[7] Wüthrich, R. (2009). *Micromachining using electrochemical discharge phenomenon-fundamentals and application of spark assisted chemical engraving.* Oxford: William Andrew Publishing.

[8] Wüthrich, R., & Mandin, P. (2009). Electrochemical discharges—Discovery and early applications. *Electrochimica Acta, 54*(16), 4031-4035.

[9] Wüthrich, R., & Bleuler, H. (2004). A model for electrode effects using percolation theory. *Electrochimica Acta, 49*(9-10), 1547-1554.

[10] Wüthrich, R., & Hof, L. A. (2006). The gas film in spark assisted chemical engraving (SACE)—A key element for micro-machining applications. *International Journal of Machine Tools and Manufacture, 46*(7-8), 828-835

[11] Krause, B., & Vogt, H. (1985). Effect of operational parameters on gas evolution in electrolyte bulk: Possibilities for lowering interelectrode resistance. *Journal of Applied Electrochemistry, 15*(4), 509-515.

[12] Boissonneau, P., & Byrne, P. (2000). An experimental investigation of bubble-induced free convection in a small electrochemical cell. *Journal of Applied Electrochemistry, 30*(7), 767-775.

[13] Bruggeman, D. A. G. (1935). The calculation of various physical constants of heterogeneous substances. I. the dielectric constants and conductivities of mixtures composed of isotropic substances. *Annalen Der Physik, 24*(7), 636-664.

[14] Maxwell, J. C. (1982). *A treatise on electricity and magnetism* (3rd ed., pp. 440)

[15] Duineveld, P. C. (1997). Bouncing and coalescence of bubble pairs rising at high reynolds number in pure water or aqueous surfactant solutions. *Applied Scientific Research, 58*(1), 409-439.

[16] Chen, L., Li, Y., & Manasseh, R. (1998). The coalescence of bubbles – A numerical study. *Proceedings of the Third International Conference Multiphase Flow,* Lyon, France. Paper 626.

[17] Prince, M. J., & Blanch, H. W. (1990). Bubble coalescence and break-up in air-sparged bubble columns. *AIChE Journal, 36*(10), 1485-1499.

[18] Fascio, V., Langen, H. H., Bleuler, H., & Comninellis, C. (2003). Investigations of the spark assisted chemical engraving. *Electrochemistry Communications, 5*(3), 203-207

[19] Hoho, P. (1894). Phénomène calorifique produit par le courant électrique au contact d'un solide et d'un liquide. *La Lumière électrique, 52*(17), 165-169.

[20] Kellogg, H. H. (1950). Anode effect in aqueous electrolysis. *Journal of the Electrochemical Society, 97*(4), 133-142.

[21] Azumi, K., Mizuno, T., Akimoto, T., & Ohmori, T. (1999). Light emission from pt during high-voltage cathodic polarization. *Journal of the Electrochemical Society, 146*(9), 3374-3377.

[22] Garbarz-Olivier, J., & Guilpin, C. (1978). The origin of the electrode effect in various electrolytes. *Journal of Electroanalytical Chemistry and Interfacial Electrochemistry, 91*(1), 79-91.

[23] Klupathy, E. (1902). Zur Theorie des Wehneltunterbrechers. *Issue Annalen der Physik Annalen der Physik, 314*(9), 147-163.

[24] Valognes, J. C., Bardet, J. P., & Mergault, P. (1987). Contribution à l'étude des effets d'électrode. *Spectrochimica Acta Part B: Atomic Spectroscopy, 42*(3), 445-458.

[25] Vogt, H. (1999). The anode effect as a fluid dynamic problem. *Journal of Applied Electrochemistry, 29*(2), 137-145.

[26] Arndt, K., & Probst, H. (1923). Untersuchungen über den Anodeneffekt. *Zeitschrift für Elektrochemie und angewandte physikalische Chemie, 29*(13-14), 323-334.

[27] Wartenberg, H. V., Versuchen, N., Manthe, E., & Conzelmann, W. (1926). Der anodeneffekt bei der schmelzflusselektrolyse. *Zeitschrift Für Elektrochemie Und Angewandte Physikalische Chemie, 32*(7), 330-336.

[28] Mazza, B., Pedeferri, P., & Re, G. (1978). Hydrodynamic instabilities in electrolytic gas evolution. *Electrochimica Acta, 23*(2), 87-93.

[29] Wüthrich, R., Comninellis, C., & Bleuler, H. (2005). Bubble evolution on vertical electrodes under extreme current densities. *Electrochimica Acta, 50*(25-26), 5242-5246.

[30] Basak, I., & Ghosh, A. (1996). Mechanism of spark generation during electrochemical discharge machining: A theoretical model and experimental verification. *Journal of Materials Processing Technology, 62*(1-3), 46-53.

[31] Sengupta, S. K., Singh, R., & Srivastava, A. K. (1998). A study on the origin of nonfaradaic behavior of anodic contact glow discharge electrolysis. *Journal of the Electrochemical Society, 145*(7), 2209-2213.

[32] Wüthrich, R. (2004). Spark assisted chemical engraving: A stochastic modeling approach. (Doctoral dissertation 2776, École Polytechnique Fédérale de Lausanne (EPFL),2003).

[33] Guilpin, C., & Garbarz-Olivier, J. (1978). Les effets d'électrodes dans les solutions aqueuses. Résultats obtenus à l'aide d'une caméra rapide. *Journal de Chimie Physique, 75*, 723-726.

[34] Cheng, C., Wu, K., Mai, C., Yang, C., Hsu, Y., & Yan, B. (2010). Study of gas film quality in electrochemical discharge machining. *International Journal of Machine Tools and Manufacture, 50*(8), 689-697.

[35] Fascio, V. (2003). Etude de la microstructuration du verre par étincelage assisté par attaque chimique: une approche electrochimique. (Dissertation Thesis 2691, École Polytechnique Fédérale de Lausanne (EPFL), 2002).

[36] Allagui, A., & Wüthrich, R. (2009). Gas film formation time and gas film life time during electrochemical discharge phenomenon. *Electrochimica Acta, 54*(23), 5336-5343.

[37] Wüthrich, R., Spaelter, U., & Bleuler, H. (2006). The current signal in spark-assisted chemical engraving (SACE): What does it tell us? *Journal of Micromechanics and Microengineering, 16*(4) 779.

[38] Fascio, V., Wüthrich, R., & Bleuler, H. (2004). Spark assisted chemical engraving in the light of electrochemistry. *Electrochimica Acta, 49*(22-23), 3997-4003.

[39] Raghuram, V., Pramila, T., Srinivasa, Y. G., & Narayanasamy, K. (1995). Effect of the circuit parameters on the electrolytes in the electrochemical discharge phenomenon. *Journal of Materials Processing Technology, 52*(2-4), 301-318.

[40] Wüthrich, R., & Allagui, A. (2010). Building micro and nanosystems with electrochemical discharges. *Electrochimica Acta, 55*(27), 8189-8196.

[41] Jalali, M., & Wüthrich, R. (2009). Improving electromagnetic shielding of composite structures with metallic nanoparticles synthesized by electrochemical discharges. *Electromagnetic Compatibility - EMC Europe, 2009 International Symposium on,* 1-4.

[42] Yonghong, L., Zhixin, J., & Jinchun, L. (1997). Study on hole machining of non-conducting ceramics by gas-filled electrodischarge and electrochemical compound machining. *Journal of Materials Processing Technology, 69*(1-3), 198-202.

[43] Daridon, A., Fascio, V., Lichtenberg, J., Wütrich, R., Langen, H., Verpoorte, E., et al. (2001). Multi-layer microfluidic glass chips for microanalytical applications. *Fresenius' Journal of Analytical Chemistry, 371*(2), 261-269.

[44] Jain, V. K., Dixit, P. M., & Pandey, P. M. (1999). On the analysis of the electrochemical spark machining process. *International Journal of Machine Tools and Manufacture, 39*(1), 165-186.

[45] Langen, H., Fascio, V., Wüthrich, R., & Viquerat, D. (2002). Three-dimensional structuring of pyrex glass devices – trajectory control. *INternational Conference of the European Society for Precision Engineering and Nanotechnology (EUSPEN),* Eindhoven. *, 2,* 435-438.

[46] Ho, K. H., & Newman, S. T. (2003). State of the art electrical discharge machining (EDM). *International Journal of Machine Tools and Manufacture, 43*(13), 1287-1300.

[47] Vogt, H. (1997). Contribution to the interpretation of the anode effect. *Electrochimica Acta, 42*(17), 2695-2705.

[48] Paulmier, T., Bell, J. M., & Fredericks, P. M. (2007). Development of a novel cathodic plasma/electrolytic deposition technique: Part 2: Physico-chemical analysis of the plasma discharge. *Surface and Coatings Technology, 201*(21), 8771-8781.

[49] Bell, J., Fredericks, P., Kiriakos, E., & Paulmier, T. (2004). A new thin film deposition process by cathodic plasma electrolysis. *Proceedings of the 28th Annual Condensed Matter and Materials Meeting,* Wagga Wagga, NSW. 2-4.

[50] Munson, B. R., Young, D. F., Okiishi, T. H., & Huebsch, W. W. (2009). Dimensional analysis, similitude, and modeling. *Fundamentals of fluid mechanics* (6th ed., pp. 332-383) John Wiley & Sons.

[51] Han, M., Min, B., & Lee, S. (2008). Modeling gas film formation in electrochemical discharge machining processes using a side-insulated electrode. *Journal of Micromechanics and Microengineering, 18*(4) 045019

[52] Zhi-Ping Zheng and Jui-Kuan Lin and Fuang-Yuan Huang,and Biing. (2008). Improving the machining efficiency in electrochemical discharge machining (ECDM) microhole drilling by offset pulse voltage. *Journal of Micromechanics and Microengineering, 18*(2) 025014.

[53] Violle, J., & Chassagny, M. (1889). Revue des travaux récents en électricité: Sur l'électrolyse. *Comptes rendus hebdomadaires des séances de l'Académie des sciences CVIII*, 284-287.

[54] Hirsh, M. N., & Oskam, H. J. (1978). *Gaseous electronics: Electrical discharges* (pp. 19) Academic Press

[55] Ghosh, A. (1997). Electrochemical discharge machining: Principle and possibilities. *Sadhana, 22*(3), 435-447

[56] Hickling, A., & Ingram, M. D. (1964). Glow-discharge electrolysis. *Journal of Electroanalytical Chemistry (1959), 8*(1), 65-81

[57] Mena, P. C., Pons, M. N., Teixeira, J. A., & Rocha, F. A. (2005). Using image analysis in the study of multiphase gas absorption. *Chemical Engineering Science, 60*(18), 5144-5150.

[58] Zaĭtsev, I., D., & Aseev, G.,G. (1992). *Properties of aqueous solutions of electrolytes* CRC Press.

[59] Gilliam, R. J., Graydon, J. W., Kirk, D. W., & Thorpe, S. J. (2007). A review of specific conductivities of potassium hydroxide solutions for various concentrations and temperatures. *International Journal of Hydrogen Energy, 32*(3), 359-364.

[60] Dutcher, C.,S., Wexler, A., S., & Clegg, S., L. *Surface tensions of inorganic multicomponent aqueous electrolyte solutions and melts* - American Chemical Society.

[61] Helmholtz, H. (1868). Über discontinuierliche flüssigkeits-bewegungen. *Monatsberichte Der Königlichen Preussische Akademie Der Wissenschaften Zu Berlin, 23*, 215-228.

[62] Taylor, G. (1950). The instability of liquid surfaces when accelerated in a direction perpendicular to their planes. *Proceedings of the Royal Society of London. Series A, Mathematical and Physical Sciences, 201.* (1065) pp. 192-196.

[63] Wehnelt, A. (1899). "Ein elektrolytischer stromunterbrecher". *Wiedemann's Ann. (Annalen Der Physik), 68*, 233